ISSN 2096-7071 (Print)
ISSN 2097-3101 (Online)
CN 10-1629/R1

CHINA CDC WEEKLY

Vol. 8 No. 21 May 22, 2026

中国疾病预防控制中心周报(英文)

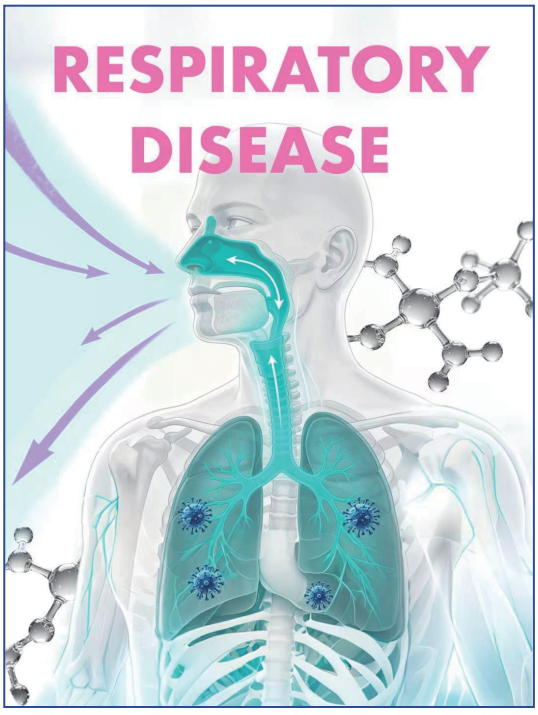

ISSN 2096-7071
9 772096 707262 21>

China CDC Weekly

Editorial Board

Editorial Office

Cover Image: credited from the designer Jiaying Wang.

Vital Surveillances

Molecular Evolution in the Second Hypervariable Region of the G Gene for Human Respiratory Syncytial Virus Lineage A.D — Worldwide, 2010–2024

Yuqing Shi[1]; Zhen Zhu[1]; Jinhua Song[1]; Naiying Mao[1]; Jie Jiang[1]; Ke Lu[1]; Na Wang[1]; Liwei Sun[2]; Linqing Zhao[3]; Yonghao Guo[4]; Ruiqiu Zhao[5]; Jiahui Xie[6]; Chao Liu[7]; Ying Chen[8]; Feng Zhang[9]; Junrui Chen[10]; Lei Cao[1]; Hongqiao Hu[1]; Baicheng Xia[1]; Yan Zhang[1,#]

ABSTRACT

Introduction: Human respiratory syncytial virus subgroup A (HRSV-A) lineage A.D is characterized by a unique 72-nucleotide duplication in the second hypervariable region of the G-gene (G-HVR2) and has become the predominant global circulating strain since 2010. Molecular evolutionary features of this region should be monitored.

Methods: A global HRSV-A G-HVR2 sequence dataset (2010–2024) was assembled that included 144 Chinese sequences and the molecular characteristics and evolutionary patterns in lineage A.D were analyzed.

Results: Molecular clock analysis based on G-HVR2 estimated that HRSV-A lineage A.D originated in 2006, with subsequent diversification into four distinct lineages. A.D.4 and A.D.5 were grouped as A.D.4/A.D.5. Lineages circulate globally with temporal fluctuations and sequential dominance shifts. The evolutionary rate of A.D was high, with the highest rate observed in A.D.4/A.D.5. Amino acid analysis indicated five shared, lineage-specific mutations in A.D.1 and A.D.4/A.D.5 that coincided with high-frequency mutation sites. Nine positively-selected sites were predicted across all lineages, three of which resided within the 72-nucleotide duplication. A.D.1 and A.D.4/A.D.5 lost conserved N- and O-glycosylation sites. A 72-nucleotide duplication in lineage A.D introduced two extra β-strands and two unique α-helical motifs relative to the prototype strain.

Conclusion: Adaptive evolution in the G-HVR2 region of HRSV-A lineage A.D was evident, likely facilitating the rapid transmission of this lineage. Sustained monitoring of lineage-specific evolution in this region is critical for targeted prevention and control of HRSV infections.

Human respiratory syncytial virus (HRSV) is the leading cause of acute lower respiratory tract infections worldwide, and it poses a substantial burden in terms of hospitalization and mortality in young children, older adults, and immunocompromised individuals (*1*). Currently, HRSV infection has become a major global public health concern.

HRSV is considered a single serotype but is divided into two antigenic subgroups: A and B (*2*). HRSV subgroup A (HRSV-A) exhibits high genetic diversity and has diversified into multiple lineages, of which lineage A.D has increased rapidly in global prevalence since its initial detection in 2010 (*3*). Whole genome analyses have classified A.D into five major lineages (A.D.1–A.D.5). A defining molecular feature of this lineage is a 72-nucleotide duplication (position: aa284–307) in the second hypervariable region of the G gene (G-HVR2) (position: aa212–321), a region characterized by high genetic variability and substantial clinical immune selection pressure (*4*).

In recent years, accumulation of G-HVR2 sequences has made it possible to comprehensively investigate their molecular characteristics and evolutionary dynamics. Therefore, we assembled a global G-HVR2 dataset for the HRSV-A lineage A.D from 2010–2024, and conducted a phylogenetic analysis, evolutionary assessment, genetic variation profiling, and structural prediction to characterize the adaptive evolution of the G-HVR2 region containing the 72-nucleotide duplication. The study aimed to provide scientific data for the targeted prevention and control of HRSV infection, as well as future investigations into its potential links with viral biological properties.

METHODS

G-HVR2 Dataset Construction

A total of 52 representative G-HVR2 sequences (National Microbiology Data Center reference

numbers: NMDCN0009ROK–NMDCN0009RQ7) of HRSV-A lineage A.D strains from nine provinces in China from 2012–2024 were included in this study (Supplementary Table S1, available at https://weekly.chinacdc.cn). After excluding sequences with incomplete targets or ambiguous temporal and geographic information, 2,402 representative G-HVR2 sequences belonging to lineage A.D from 30 countries (2010–2024) were downloaded from GenBank (version 264.0; https://www.ncbi.nlm.nih.gov/genbank/; December 2024; National Center for Biotechnology Information, Bethesda, MD, USA) based on sequence divergence and spatiotemporal characteristics. The integration of these sequences yielded a comprehensive database comprising 2,454 G-HVR2 sequences of the HRSV-A lineage A.D for subsequent analysis, which included 144 Chinese sequences from 16 provinces (2010–2024).

Phylogenetic and Molecular Evolutionary Analysis

Sequences were aligned using MAFFT (version 7.490; Osaka University, Osaka, Japan). A maximum likelihood (ML) phylogenetic tree was constructed using MEGA (version 11; Pennsylvania State University, State College, PA, USA) (GTR+F+R4 model, 1,000 bootstraps) and visualized using the online tool, iTOL (version 7.5.1; https://itol.embl.de/; April 2025; European Molecular Biology Laboratory, Heidelberg, Germany). Furthermore, 199 representative A.D lineage sequences from 28 countries were selected for molecular evolutionary analysis. Bayesian phylogenetic inference was conducted using BEAST (version 1.10.4; University of Auckland, Auckland, New Zealand) (Strict clock model, coalescent-based Bayesian skyline plot). Temporal signals were assessed using root-to-tip regression in TempEst (version 1.5.3; University of Edinburgh, Edinburgh, UK), and the best-fit model was selected using jModelTest (version 2.1.6; University of Vigo, Vigo, Spain). Evolutionary rates and time to the most recent common ancestor (tMRCA) were estimated, and population dynamics were reconstructed using Bayesian skyline plot (BSP) analysis in Tracer (version 1.7.2; University of Auckland, Auckland, New Zealand).

Genetic Variation, Selection Pressure Analysis, and Glycosylation Site Prediction

Amino acid variations were analyzed using MEGA 11, with lineage-specific mutations defined as those with >80% frequency relative to the A.D prototype strain (GenBank accession number: JN257693). High-frequency mutation sites (>60%) were identified with entropy analysis using BioEdit (version 7.2.5; North Carolina State University, Raleigh, NC, USA). Selection pressures were assessed using FUBAR, MEME, and SLAC on Datamonkey (version 2.0; https://www.datamonkey.org/; Temple University, Philadelphia, PA, USA), with positive selection (dN/dS >1) defined as $P<0.05$ or posterior probability >0.95, requiring support from at least two methods. Potential N- and O-glycosylation sites were predicted using NetNGlyc 1.0 and NetOGlyc 4.0 (https://services.healthtech.dtu.dk/services; Technical University of Denmark, Lyngby, Denmark) servers, respectively.

Protein Structural Prediction

Using the A.D prototype strain as a reference, the identified lineage-specific mutations and positive selection sites were mapped onto the predicted secondary structure of the G protein using PSIPRED (version 4.0; https://bioinf.cs.ucl.ac.uk/psipred/; University College London, London, UK) to evaluate their potential impacts.

RESULTS

Phylogenetic Classification of Lineage A.D Based on G-HVR2

Phylogenetic analysis showed that 2,454 A.D sequences could be subdivided into four distinct lineages based on G-HVR2, largely consistent with the novel genotype classification (A.D.1–A.D.5) based on whole genome sequences (*5*). However, the highly genetically related strains, A.D.4 and A.D.5, as defined in the whole genome genotyping method, were topologically indistinguishable in G-HVR2 analysis and thus grouped as 'A.D.4/A.D.5' in the current study. The proportions of the four A.D lineages in the database were similar: A.D.1 (763 strains, 31.1%), A.D.2 (501 strains, 20.4%), A.D.3 (698 strains, 28.4%), and A.D.4/A.D.5 (492 strains, 20.1%) (Supplementary Table S2, available at https://weekly.chinacdc.cn). Based on the G-HVR2 region, the average genetic distance across all A.D lineages was 0.04. The inter-lineage distances were 0.037–0.048, and the maximum intra-lineage distance was 0.035 (Supplementary Table S3, available at https://weekly.chinacdc.cn).

Prevalence Patterns of Four A.D Lineages

A global epidemic pattern analysis indicated that four A.D lineages co-circulated from 2010 to 2024, each exhibiting a broad geographical distribution. However, their detection rates varied across the years. Lineage A.D.1 emerged as the dominant strain from 2018 onwards, peaking at 46.52% in 2020. Lineage A.D.2 accounted for a substantial proportion (12.50%–58.57%) from 2013–2020 and became dominant in 2017. Lineage A.D.3 was predominant from 2010–2016 (42.11%–100%) and re-emerged as the dominant lineage in 2024 (43.59%). Lineage A.D.4/A.D.5 dominated between 2021 and 2023, with detection rates of 35.91%–50.35% (Figure 1).

All four lineages were detected in China, each showing a distinct spatiotemporal pattern. Lineages A.D.2 (16.7%, six provinces) and A.D.3 (73.6%, 11 provinces) were detected from 2012–2020 and 2012–2024, respectively. Since 2018, lineages A.D.1 (5.5%, six provinces, 2019–2023) and A.D.4/A.D.5 (4.2%, five provinces, 2018–2023) were successively identified. Consistent with global patterns, A.D.2 (46.67%–50.00%) and A.D.3 (50.00%–100%) dominated from 2011–2017, with A.D.3 being the most frequent lineage during this period. Since 2018, A.D.3 has been predominant (57.14%–100%), except

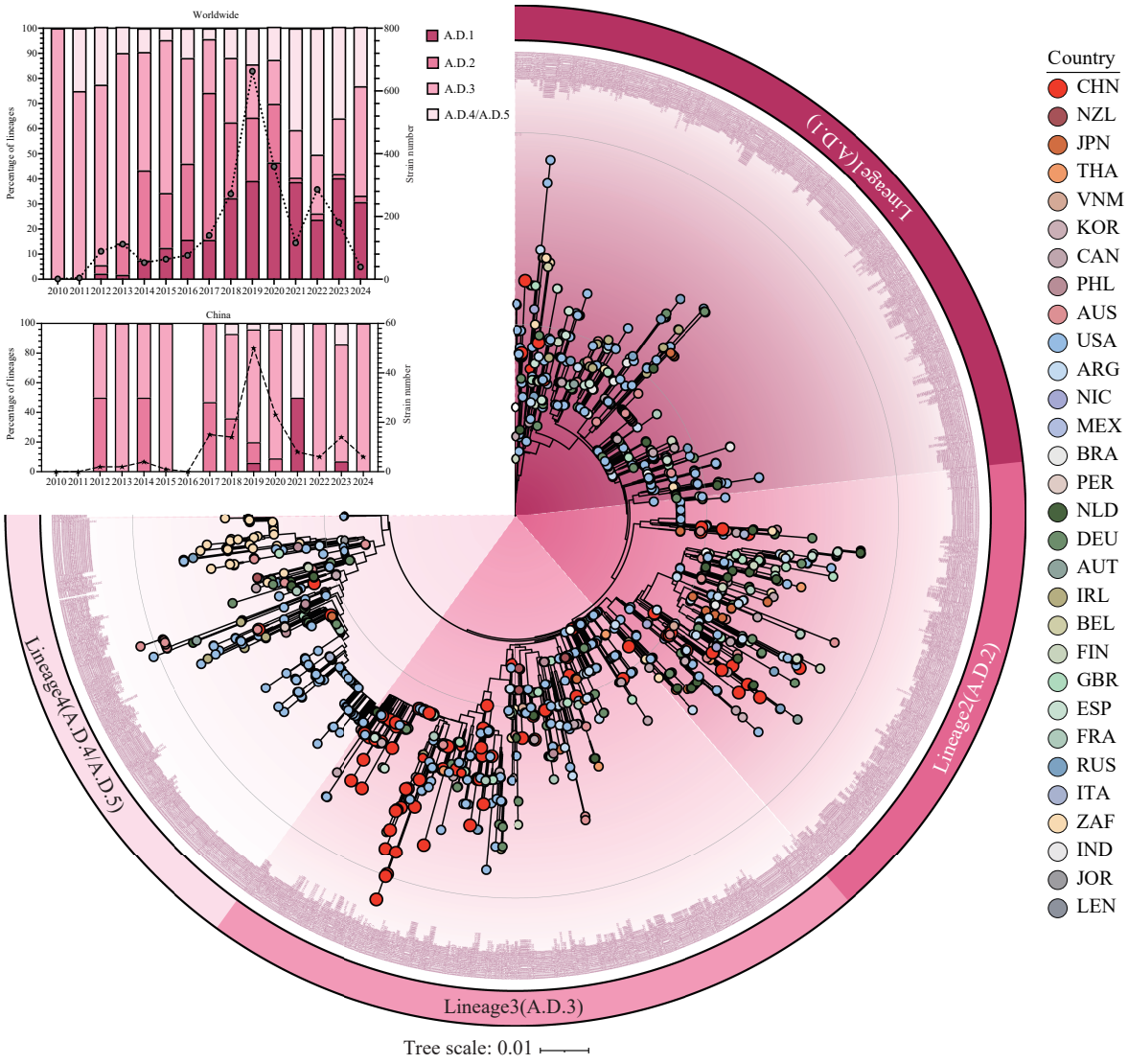

FIGURE 1. Phylogenetic and spatiotemporal distribution of 2,454 HRSV-A lineage A.D sequences.
Note: The upper-right panel presents the maximum likelihood phylogenetic tree constructed based on G-HVR2. The outer ring indicates the lineage classification (Lineages A.D.1–A.D.4/A.D.5). The upper-left panel illustrates the prevalence of the four lineages in China and worldwide.
Abbreviation: HRSV-A=human respiratory syncytial virus subgroup A; G-HVR2=second hypervariable region of the G gene.

in 2021 when only A.D.1 (50.00%) and A.D.4/A.D.5 (50.00%) were detected and aligned with global lineages circulating at that time (Figure 1).

Molecular Evolution of Lineage A.D

Based on the representative sequences, root-to-tip regression analysis indicated a strong temporal signal with a correlation coefficient =0.9987 and R^2=0.9974 (Figure 2). The overall estimated evolutionary rate for lineage A.D was 5.63×10^{-3} substitutions/site/year (95% highest posterior density (HPD): 1.00×10^{-3} to 11.28×10^{-3}), with tMRCA estimated to be approximately 2006 (95% HPD: 2005–2010). The evolutionary rates of the four lineages varied from 1.92×10^{-3} (95% HPD: 4.18×10^{-6} to 6.36×10^{-3}) to 5.26×10^{-3} substitutions/site/year (95% HPD: 1.93×10^{-5} to 13.01×10^{-3}), with the highest rate in lineage A.D.4/A.D.5. The tMRCAs for these lineages were similar, and they occurred between 2008 and 2009(SupplementaryTableS4,availableathttps://weekly.chinacdc.cn). Furthermore, BSP analysis indicated that lineage A.D underwent a rapid and pronounced expansion in effective population size between 2010 and 2012, followed by a period of relative stability (Figure 2).

Amino Acid Variation and Selective Pressure Analysis of A.D Lineages

Compared to the A.D prototype strain, lineage-specific mutations in G-HVR2 were identified: A.D.1 had four sites (L274P, L298P, Y304H, T320A), and A.D.4/A.D.5 had two mutations (Y304H and L310P), with Y304H being a shared mutation between the two lineages. No lineage-specific mutations were detected in A.D.2 or A.D.3 (Figure 3A). Entropy analysis indicated five high-frequency mutations in G-HVR2 (aa274, aa298, aa304, aa319, and aa320). Four of these (excluding aa319) corresponded to lineage-specific mutations and two (aa298 and aa304) were located within a 72-nucleotide duplication. Selection pressure analysis indicated nine sites under positive selection across A.D lineages: three in A.D.1 (aa214, aa255, aa314), five in A.D.2 (aa273, aa297, aa298, aa309, and aa314), three in A.D.3 (aa274, aa297, aa298), and three in A.D.4/A.D.5 (aa273, aa284, aa297). Notably, aa284, aa297, and aa298 were located in the 72-nucleotide duplication (Figure 3B).

Glycosylation Site Prediction

Glycosylation site prediction identified two N-glycosylation sites (aa237 and aa318) in the G-HVR2 of A.D lineages. A.D.1 and A.D.4/A.D.5 lost their N-glycosylation site at aa318. No N-glycosylation sites were found in the 72-nucleotide duplications. Additionally, the A.D lineages contained 43 O-glycosylation sites in G-HVR2, 10 of which were located in the 72-nucleotide duplication. However, A.D.1 lost one O-glycosylation site at aa320, and A.D.4/A.D.5 had deletions at aa305, aa319, and aa320 (Figure 3C).

Structural Prediction

The DMPFold structural prediction results indicated that the 72-nucleotide duplication at the C-terminus of G protein induced the formation of a coiled conformation, introducing two extra β-strands and two unique α-helical motifs relative to the prototype strain of HRSV-A (Figure 4A). However, the identified lineage-specific mutations did not lead to observable changes in the protein conformation (Figure 4B).

DISCUSSION

The HRSV-A lineage A.D, characterized by a 72-nucleotide duplication in G-HVR2, has rapidly become the predominant strain circulating globally over the past decade (*6*). Molecular clock analyses estimated that lineage A.D originated in 2006 (*7*). This lineage subsequently diversified into multiple distinct lineages (A.D.1–A.D.4/A.D.5) occurring between 2008 and 2009. After a period of covert transmission, a rapid and substantial expansion in the effective population size of lineage A.D was observed between 2010 and 2012 using BSP analysis, suggesting lineage-specific adaptive evolution of A.D within the human population. This process may be driven by multiple factors, such as amino acid mutations, glycosylation site alterations, and conformational changes in G-HVR2.

Prevalence trend analysis showed that the A.D lineages (A.D.1–A.D.4/A.D.5) subsequently circulated worldwide with marked temporal fluctuations and successive dominance shifts. This sequential dominance pattern possibly reflects the combined effects of interlineage competition, immune-mediated selection, and coronavirus disease 2019-related public health interventions (*8*). Circulation patterns in China largely paralleled global patterns but exhibited distinct regional features, with A.D.3 maintaining a

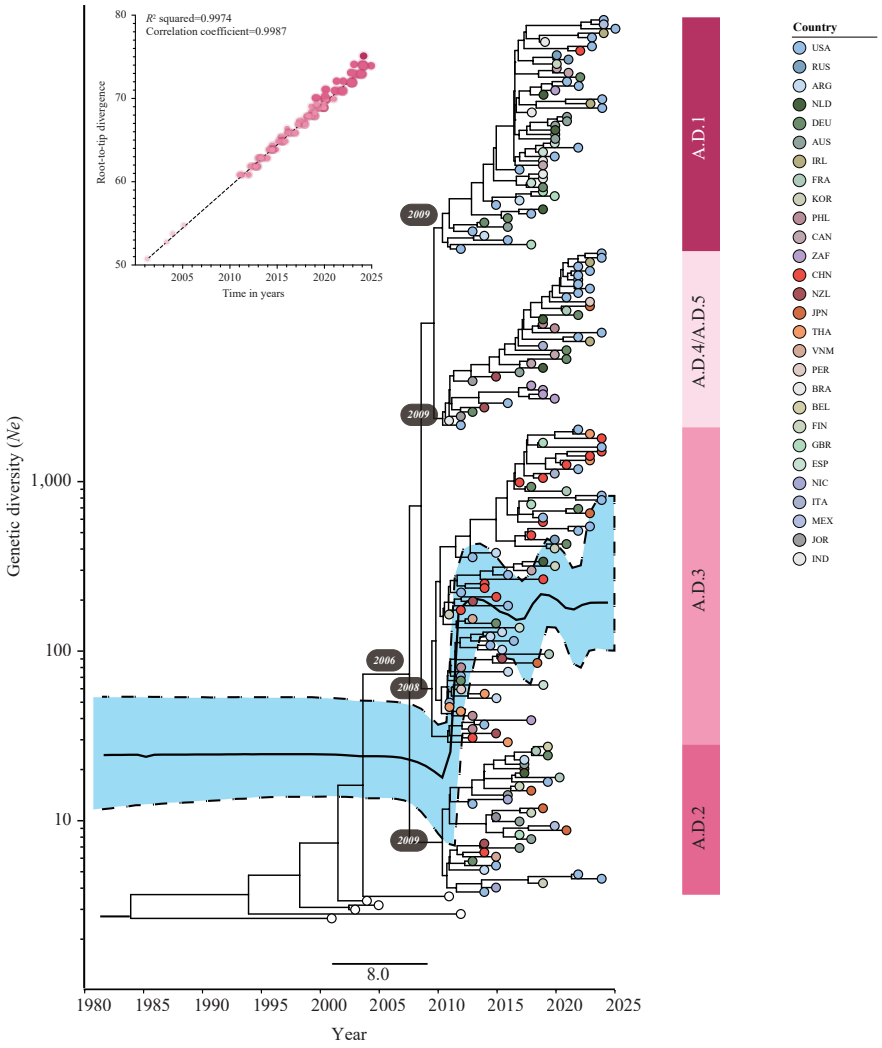

FIGURE 2. Time-scaled phylogeny and evolutionary dynamics of 199 HRSV-A lineage A.D and six reference sequences from other lineages (A.1–A.3).
Note: A maximum clade credibility tree was constructed based on G-HVR2. The scatter plot on the upper left shows the results of the root-to-tip regression analysis. The diagram embedded in the tree represents a Bayesian skyline plot. The vertical axis indicates the effective population size, and the horizontal axis represents the year. The representative strains corresponding to the unlabeled branches in the figure are A.1–A.3 representative strains.
Abbreviation: HRSV-A=human respiratory syncytial virus subgroup A; G-HVR2=second hypervariable region of the G gene.

consistently high prevalence across most years, highlighting regional heterogeneity in lineage adaptation and transmission dynamics. Therefore, continuous lineage-related surveillance is crucial to understand the global prevalence and evolutionary patterns of HRSV-A (*9*).

Molecular evolutionary analysis based on G-HVR2 indicated a high overall evolutionary rate for A.D lineages (5.63×10^{-3} substitutions/site/year), which was consistent with previous findings (*10*). Of the four lineages, A.D.4/A.D.5 exhibited the highest rate. Moreover, lineage-specific mutations in A.D.1 and A.D.4/A.D.5 overlapped substantially with high-frequency mutation sites, suggesting that these genetic changes might be attributed to the adaptive evolution associated with its recent emergence as a dominant strain (*11*).

Selection pressure analysis identified nine positively-selected sites across all lineages, three of which (aa284, aa297, and aa298) were located within the 72-nucleotide duplication, indicating that lineage-defining residues in G-HVR2 were strongly targeted by positive selection. Several duplication sites exhibited concurrent high-frequency variations and lineage-specific changes. For example, residue 298 was positively selected in A.D.2 and A.D.3, whereas in A.D.1, it represented a

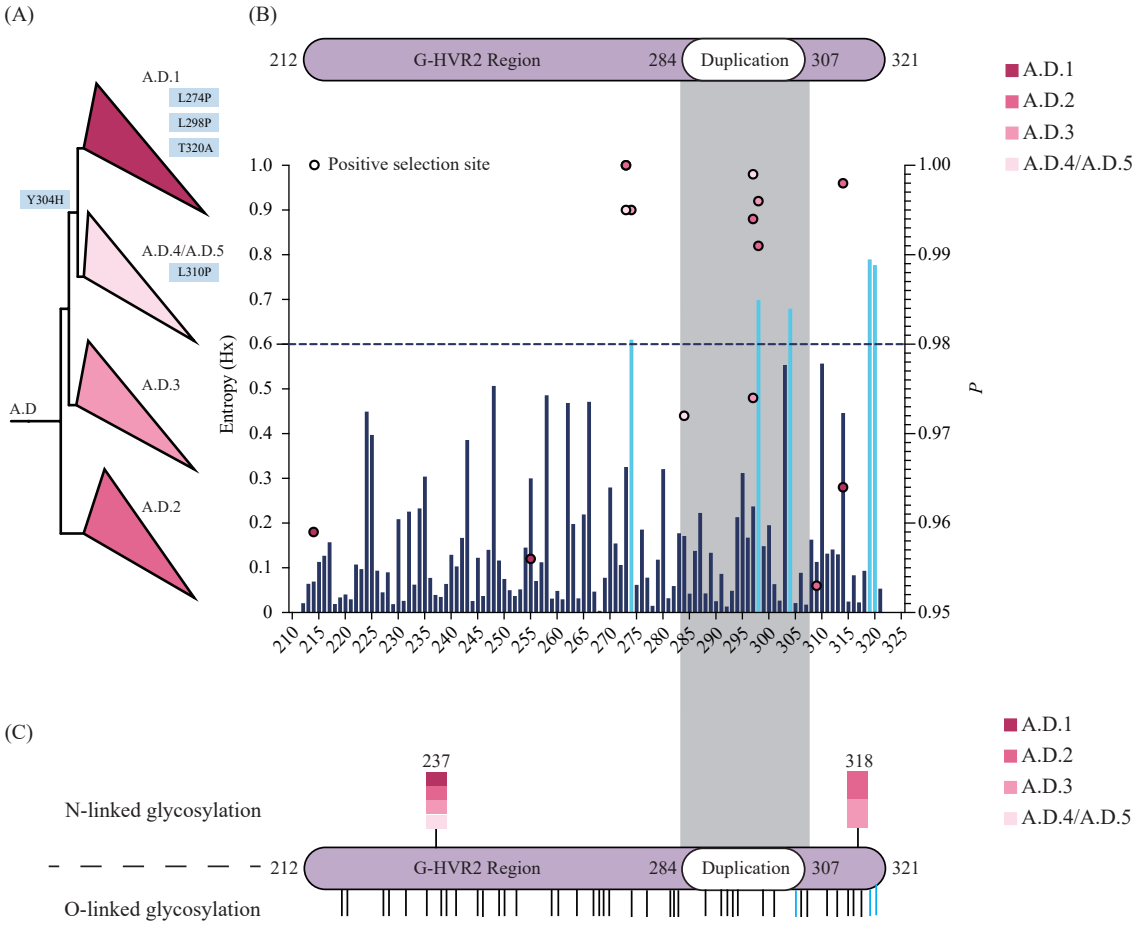

FIGURE 3. Lineage-specific amino acid sites, entropy analysis, selective pressure, and glycosylation of the HRSV-A A.D lineages based on G-HVR2. (A) Lineage-specific amino acid sites. (B) Entropy analysis and predicted positively-selected sites. (C) Predicted N- and O-linked glycosylation sites.

Note: For (A), a schematic phylogenetic tree displaying color-coded lineages and lineage-specific amino acid sites highlighted in blue boxes. For (B), the schematic presents the G-HVR2 region, in which the 72-nucleotide duplication is highlighted with gray shading. Entropy analysis identified high-frequency mutation sites (vertical axis, entropy; horizontal axis, amino acid position); those exceeding an entropy of 0.6 are displayed in light-blue, and predicted positively-selected sites are marked by circles whose colors correspond to different lineages. For (C), sites including predicted N-glycosylation sites are presented in the upper panel, with colors indicating different lineages; predicted O-glycosylation sites are in the lower panel, where vertical lines denote site positions and blue lines show O-glycosylation sites specific to lineages A.D.2 and A.D.3.

Abbreviation: HRSV-A=human respiratory syncytial virus subgroup A; G-HVR2=second hypervariable region of the G gene.

lineage-specific L298P substitution and a high-frequency variant. These findings were consistent with those of previous studies (*12–13*), supporting the critical role of the 72-nucleotide duplication in G-HVR2 in HRSV-A immune evasion and adaptive evolution.

In addition to the shared Y304H mutation, A.D.1 and A.D.4/A.D.5 exhibited a concurrent loss of conserved N- and O-linked glycosylation sites, indicating a convergent adaptive advantage in these lineages. Altered glycosylation patterns may affect protein conformational stability, immunogenicity, or receptor-binding properties, potentially shaping the phenotypic and epidemiological profiles of distinct viral lineages (*14–15*). Given the increasing global detection rates of A.D.1 and A.D.4/A.D.5 in recent years, it has become imperative to elucidate the potential link between glycosylation changes and disease burden or clinical phenotypes.

Secondary structure prediction indicated that, compared to the HRSV-A prototype strain (lineage A.1), the G protein of lineage A.D contained a duplication insertion that introduced two additional β-strands and two unique α-helical motifs. This

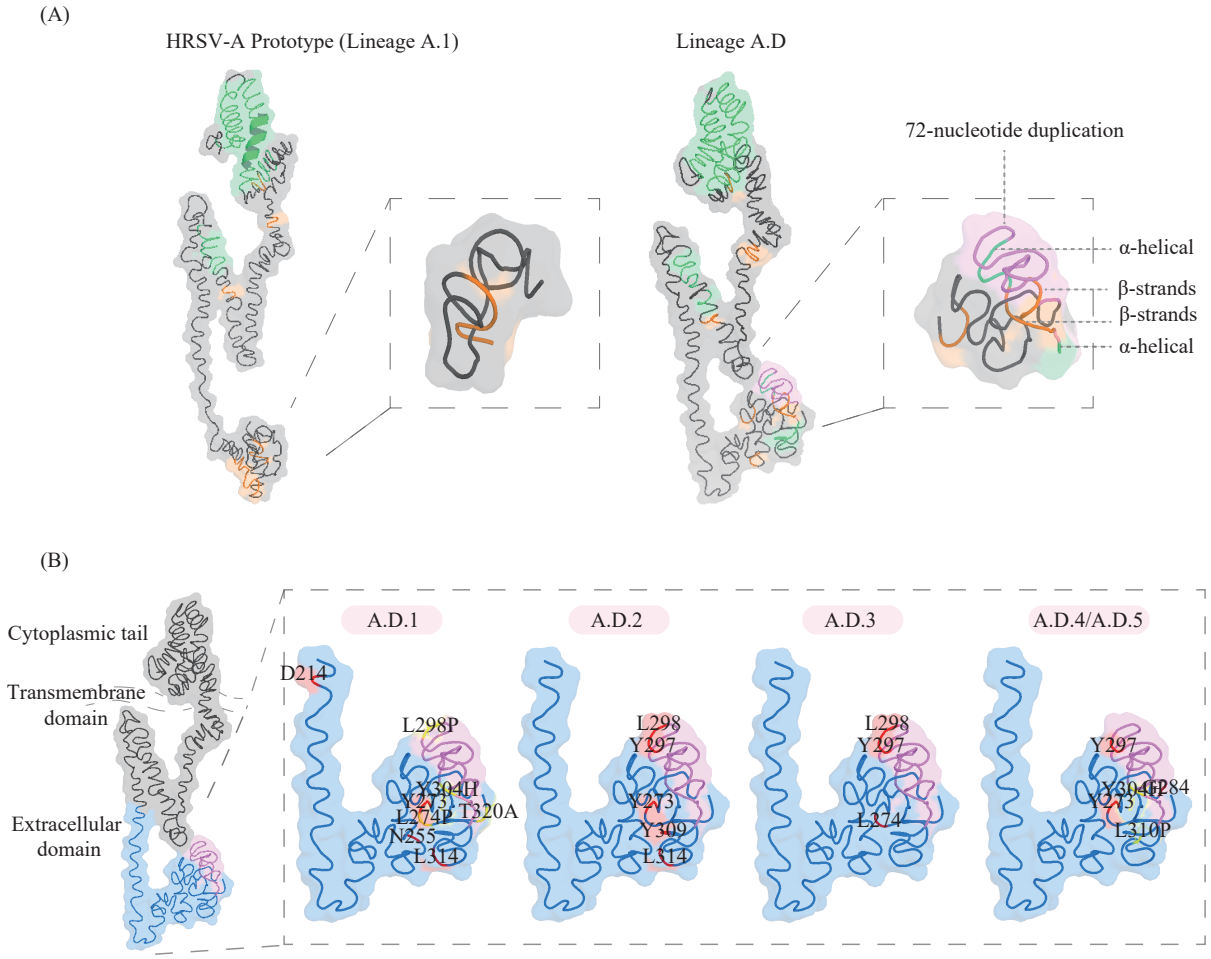

FIGURE 4. Secondary structure prediction of HRSV-A G protein. (A) Comparison of the G protein secondary structure between the HRSV-A prototype strain and lineage A.D. (B) Predicted secondary structures of the G protein in different A.D lineages.

Note: For (A), on the left is the secondary structure of the G protein from the HRSV-A prototype strain. On the right is the secondary structure of the G protein from A.D lineages, in which the α-helices and β-sheets introduced by the duplicated insertion are colored green and yellow, respectively. For (B), the G-HVR2 region is highlighted in blue, the 72-nucleotide duplication is shown in pink, lineage-specific sites are marked with a yellow background, and positively selected sites are indicated by a red background.

Abbreviation: HRSV-A=human respiratory syncytial virus subgroup A; G-HVR2=second hypervariable region of the G gene.

structural remodeling may alter G protein binding to host cell receptors and the immunorecognition of conformational epitopes. However, due to the high degree of glycosylation in G proteins, the choice of modeling framework might influence the structural prediction results; thus, such structural changes require further validation.

The findings of this study highlighted that the G-HVR2 occupied a significant position in the sustained adaptive evolution of HRSV-A lineage A.D. This study employed a reverse genetics platform to conduct functional validation of this duplication, enabling direct assessment of its biological characteristics. Preliminary data (unpublished) revealed that the duplication exerted a substantial influence on viral pathogenicity, underscoring its potential contribution to lineage-specific adaptation.

Limitations of this study: First, compared with whole-genome analysis, lineage division based on the G-HVR2 lacks sufficient resolution to reliably distinguish closely related A.D.4 and A.D.5. Second, the paucity of available Chinese sequence data might lead to underestimation of the circulation of lineages. Third, the findings might be subject to potential influence from insufficient surveillance or sampling bias.

In conclusion, this study delineated the prevalence and transmission dynamics of the currently dominant

HRSV-A lineage A.D. Systematic analysis of genetic polymorphisms, selective pressures, glycosylation patterns, and structural predictions demonstrated significant adaptive evolution in the G-HVR2 region containing a 72-nucleotide duplication, which likely facilitated the lineage's rapid transmission. Accordingly, ongoing monitoring of lineage-specific genetic evolution in this region is critical for targeted prevention and control of HRSV infection.

Conflicts of interest: The authors declare no conflicts of interest.

Funding: Supported by the Beijing Natural Science Foundation (Grant No. L252073).

doi: 10.46234/ccdcw2026.103

[#] Corresponding author: Zhang Yan, zhangyan@ivdc.chinacdc.cn.

[1] National Key Laboratory of Intelligent Tracking and Forecasting for Infectious Diseases, NHC Key Laboratory of Medical Virology and Viral Disease, National Institute for Viral Disease Control and Prevention, Chinese Center for Disease Control and Prevention & Chinese Academy of Preventive Medicine, Beijing, China; [2] Children's Hospital of Changchun, Changchun City, Jilin Province, China; [3] Laboratory of Virology, Beijing Key Laboratory of Etiology of Viral Diseases in Children, Capital Institute of Pediatrics, Beijing, China; [4] Henan Provincial Center for Disease Control and Prevention, Zhengzhou City, Henan Province, China; [5] Department of Infectious Diseases, Children's Hospital Affiliated to Chongqing Medical University, Chongqing, China; [6] Master's Degree Virus Laboratory, Guangzhou Women and Children's Medical Center, Guangzhou Medical University, Guangzhou City, Guangdong Province, China; [7] Shenyang Center for Disease Control and Prevention (Shenyang Health Inspection Institute), Shenyang City, Liaoning Province, China; [8] Inner Mongolia Autonomous Region Academy of Preventive Medicine, Inner Mongolia Autonomous Region Center for Disease Control and Prevention, Hohhot City, Inner Mongolia Autonomous Region, China; [9] Laboratory of Viral Diseases, Qingdao Municipal Centre for Disease Control and Prevention, Qingdao Institute of Prevention Medicine, Qingdao City, Shandong Province, China; [10] Jining Medical University, Jining City, Shandong Province, China.

Submitted: April 02, 2026
Accepted: May 13, 2026
Issued: May 22, 2026

REFERENCES

1. Wang X, Li Y, Shi T, Bont LJ, Chu HY, Zar HJ, et al. Global disease burden of and risk factors for acute lower respiratory infections caused by respiratory syncytial virus in preterm infants and young children in 2019: a systematic review and meta-analysis of aggregated and individual participant data. Lancet 2024;403(10433):1241 – 53. https://doi.org/10.1016/S0140-6736(24)00138-7.
2. Mufson MA, Örvell C, Rafnar B, Norrby E. Two distinct subtypes of human respiratory syncytial virus. J Gen Virol 1985;66(Pt 10):2111-24. http://dx.doi.org/10.1099/0022-1317-66-10-2111.
3. Langedijk AC, Vrancken B, Lebbink RJ, Wilkins D, Kelly EJ, Baraldi E, et al. The genomic evolutionary dynamics and global circulation patterns of respiratory syncytial virus. Nat Commun 2024;15(1):3083. https://doi.org/10.1038/s41467-024-47118-6.
4. Eshaghi A, Duvvuri VR, Lai R, Nadarajah JT, Li AM, Patel SN, et al. Genetic variability of human respiratory syncytial virus A strains circulating in Ontario: a novel genotype with a 72 nucleotide G gene duplication. PLoS One 2012;7(3):e32807. https://doi.org/10.1371/journal.pone.0032807.
5. Goya S, Ruis C, Neher RA, Meijer A, Aziz A, Hinrichs AS, et al. Standardized phylogenetic classification of human respiratory syncytial virus below the subgroup level. Emerg Infect Dis 2024;30(8):1631 – 41. https://doi.org/10.3201/eid3008.240209.
6. Cantú-Flores K, Rivera-Alfaro G, Muñoz-Escalante JC, Noyola DE. Global distribution of respiratory syncytial virus A and B infections: a systematic review. Pathog Glob Health 2022;116(7):398 – 409. https://doi.org/10.1080/20477724.2022.2038053.
7. Yu JM, Fu YH, Peng XL, Zheng YP, He JS. Genetic diversity and molecular evolution of human respiratory syncytial virus A and B. Sci Rep 2021;11(1):12941. https://doi.org/10.1038/s41598-021-92435-1.
8. Guo CY, Zhang Y, Zhang YY, Zhao W, Peng XL, Zheng YP, et al. Comparative analysis of human respiratory syncytial virus evolutionary patterns during the COVID-19 pandemic and pre-pandemic periods. Front Microbiol 2023;14:1298026. https://doi.org/10.3389/fmicb.2023.1298026.
9. Song JJ, Zhu Z, Song JH, Mao NY, Cui AL, Xu WB, et al. Circulation pattern and genetic variation of human respiratory syncytial virus in China during 2008-2021. J Med Virol 2023;95(3):e28611. https://doi.org/10.1002/jmv.28611.
10. Yan B, Wang JF, Xu CD, Liu J. Spatial transmission dynamics of respiratory syncytial virus A in China. Transbound Emerg Dis 2025;2025(1):9926198. https://doi.org/10.1155/tbed/9926198.
11. Zhuang TX, Fall A, Norton JM, Abdullah O, Villafuerte DA, Pekosz A, et al. Whole-genome sequence characterization of respiratory syncytial virus in the Johns Hopkins Health System during the 2024–2025 respiratory season. Microbiol Spectr 2025;13(11):e02065 – 25. https://doi.org/10.1128/spectrum.02065-25.
12. Bergeron HC, Murray J, Arora A, Castrejon AMN, DuBois RM, Anderson LJ, et al. Immune prophylaxis targeting the respiratory syncytial virus (RSV) G protein. Viruses 2023;15(5):1067. https://doi.org/10.3390/v15051067.
13. Botosso VF, De A Zanotto PM, Ueda M, Arruda E, Gilio AE, Vieira SE, et al. Positive selection results in frequent reversible amino acid replacements in the G protein gene of human respiratory syncytial virus. PLoS Pathog 2009;5(1):e1000254. https://doi.org/10.1371/journal.ppat.1000254.
14. García-Beato R, Melero JA. The C-terminal third of human respiratory syncytial virus attachment (G) protein is partially resistant to protease digestion and is glycosylated in a cell-type-specific manner. J Gen Virol 2000;81(Pt 4):919-27. http://dx.doi.org/10.1099/0022-1317-81-4-919.
15. Fuentes S, Coyle EM, Golding H, Khurana S. Nonglycosylated G-protein vaccine protects against homologous and heterologous respiratory syncytial virus (RSV) challenge, while glycosylated G enhances RSV lung pathology and cytokine levels. J Virol 2015;89(16):8193 – 205. https://doi.org/10.1128/JVI.00133-15.

SUPPLEMENTARY MATERIAL

SUPPLEMENTARY TABLE S1. List of the 52 G-HVR2 sequences in this study.

No. strain	Year	PLAD	NMDC number	No. strain	Year	PLAD	NMDC number
Changchun12-10	2012	Jilin	NMDCN0009ROK	JL-01-2021-934	2021	Jilin	NMDCN0009RPE
Changchun13-12	2013	Jilin	NMDCN0009ROL	JL-01-2021-841	2021	Jilin	NMDCN0009RPF
Changchun14-52	2014	Jilin	NMDCN0009ROM	JL-01-2021-830	2021	Jilin	NMDCN0009RPG
HeN17-21	2017	Henan	NMDCN0009RON	BJ-01-2021-315	2021	Beijing	NMDCN0009RPH
HeN17-18	2017	Henan	NMDCN0009ROO	JL-01-2022-54	2022	Jilin	NMDCN0009RPI
HeN17-15	2017	Henan	NMDCN0009ROP	JL-01-2022-133	2022	Jilin	NMDCN0009RPJ
HeN17-09	2017	Henan	NMDCN0009ROQ	JL-01-2022-103	2022	Jilin	NMDCN0009RPK
HeN17-05	2017	Henan	NMDCN0009ROR	CQ-01-2022-19	2022	Chongqing	NMDCN0009RPL
HeN17-01	2017	Henan	NMDCN0009ROS	CQ-01-2022-10	2022	Chongqing	NMDCN0009RPM
BJ17-29	2017	Beijing	NMDCN0009ROT	BJ-02-2023-139	2023	Beijing	NMDCN0009RPN
BJ17-11	2017	Beijing	NMDCN0009ROU	JL-01-2023-635	2023	Jilin	NMDCN0009RPO
BJ17-08	2017	Beijing	NMDCN0009ROV	HN-01-2023461	2023	Henan	NMDCN0009RPP
BJ17-02	2017	Beijing	NMDCN0009RP0	GD-01-2023-97	2023	Guangdong	NMDCN0009RPQ
HeN18-08	2018	Henan	NMDCN0009RP1	GD-01-2023-210	2023	Guangdong	NMDCN0009RPR
HeN18-03	2018	Henan	NMDCN0009RP2	CQ-01-2023149	2023	Chongqing	NMDCN0009RPS
BJ18-03	2018	Beijing	NMDCN0009RP3	CQ-01-2023129	2023	Chongqing	NMDCN0009RPT
BJ18-02	2018	Beijing	NMDCN0009RP4	CQ-01-2023-072	2023	Chongqing	NMDCN0009RPU
SH19-11	2019	Shanghai	NMDCN0009RP5	CQ-01-2023-034	2023	Chongqing	NMDCN0009RPV
SH19-10	2019	Shanghai	NMDCN0009RP6	CQ-01-2023-031	2023	Chongqing	NMDCN0009RQ0
SH19-08	2019	Shanghai	NMDCN0009RP7	BJ-02-2023-323	2023	Beijing	NMDCN0009RQ1
BJ19-07	2019	Beijing	NMDCN0009RP8	BJ-02-2023-311	2023	Beijing	NMDCN0009RQ2
BJ19-03	2019	Beijing	NMDCN0009RP9	BJ-02-2023-100	2023	Beijing	NMDCN0009RQ3
SD-01-2021-291	2021	Shandong	NMDCN0009RPA	JL-01-2024-67	2024	Jilin	NMDCN0009RQ4
NM01-2021-14	2021	Inner Mongolia	NMDCN0009RPB	JL-01-2024-35	2024	Jilin	NMDCN0009RQ5
LN-01-2021-078	2021	Liaoning	NMDCN0009RPC	JL01-2024-303	2024	Jilin	NMDCN0009RQ6
JL-01-2021-936	2021	Jilin	NMDCN0009RPD	GD-02-2024018	2024	Guangdong	NMDCN0009RQ7

Abbreviation: G-HVR2=second hypervariable region of the G gene; PLAD=provincial-level administrative division; NMDC=national microbiome data collaborative.

SUPPLEMENTARY TABLE S2. The spatiotemporal distribution of four A.D lineages.

Lineages	Global distribution			Distribution in China			
	No. of strains	No. of countries	Period	No. of strains	No. of PLADs	Period	Distribution by PLAD
A.D.1	763	21	2012–2024	8	6	2019; 2021; 2023	Beijing; Shanghai; Shandong; Jilin; Liaoning; Inner Mongolia; Taiwan
A.D.2	501	27	2012–2024	24	6	2012; 2014; 2017–2020	Beijing; Hubei; Henan, Shanghai; Shandong; Zhejiang; Jiangsu
A.D.3	698	25	2010–2024	106	11	2012–2015; 2017–2020; 2021–2024	Beijing; Jilin; Henan; Shanghai; Guangdong; Zhejiang; Taiwan; Chongqing; Gansu; Ningxia; Yunnan
A.D.4/ A.D.5	492	22	2011–2024	6	5	2018; 2021; 2023	Beijing; Henan; Guangdong; Zhejiang; Taiwan

Abbreviation: NMDC=national microbiome data collaborative.

SUPPLEMENTARY TABLE S3. Inter- and intra-lineage nucleotide and amino acid genetic distances for the four lineages of A.D.

Lineages	A.D.1	A.D.2	A.D.3	A.D.4/A.D.5
A.D.1	0.027/aa0.076*	0.086	0.074	0.093
A.D.2	0.037	0.035/aa0.052*	0.084	0.121
A.D.3	0.037	0.040	0.027/aa0.051*	0.111
A.D.4/A.D.5	0.040	0.048	0.045	0.028/aa0.060*
Overall		0.040/aa0.083		

Note: Interlineage genetic distances based on nucleotide sequences are presented in the lower-left region, whereas those based on amino acid sequences are displayed in the upper-right region.
Abbreviation: aa=amino acid.
* The values represent intra-lineage genetic distances.

SUPPLEMENTARY TABLE S4. The estimated evolutionary rate and tMRCA of A.D lineages.

Lineage	Evolutionary rate (95% HPD)	tMRCA (95% HPD)
A.D	5.63×10^{-3} (1.00×10^{-3}, 11.28×10^{-3})	2006 (2005, 2010)
A.D.1	2.66×10^{-3} (3.12×10^{-6}, 7.29×10^{-3})	2009 (2009, 2011)
A.D.2	4.14×10^{-3} (5.01×10^{-5}, 10.89×10^{-3})	2009 (2009, 2011)
A.D.3	1.92×10^{-3} (4.18×10^{-6}, 6.36×10^{-3})	2008 (2008, 2011)
A.D.4/A.D.5	5.26×10^{-3} (1.93×10^{-5}, 13.01×10^{-3})	2009 (2009, 2011)

Abbreviation: HPD=highest posterior density; tMRCA=the most recent common ancestor.

Preplanned Studies

Longitudinal Study of Subsequent Wheezing/Asthma Risk Among Children Hospitalized for Acute Respiratory Infections — Yichang City, Hubei Province, China, 2017–2024

Qiuyan Qin[1]; Qiqi Wang[1]; Siyu Wang[1]; Lei Wang[2]; Jinfang Sun[1,#]; Guoxing Li[3,#]

Summary

What is already known about this topic?

Severe respiratory infections in early life, particularly lower respiratory tract infections, such as bronchiolitis and pneumonia, may increase the risk of subsequent wheezing and asthma.

What is added by this report?

Among the 22,460 children hospitalized for acute respiratory infections in Yichang, 2017–2024, a total of 1,463 subsequently developed wheezing/asthma. Bronchiolitis and pneumonia were associated with the highest subsequent wheezing/asthma risk relative to upper respiratory tract infection or influenza, with excess risk concentrated within the first 2 years after hospitalization; only bronchiolitis remained significantly associated with subsequent wheezing/asthma during the 2 to <4 years period.

What are the implications for public health practice?

Children hospitalized with bronchiolitis or pneumonia should undergo systematic post-discharge follow-up and early asthma screening during the first two years after discharge. Extended follow-up for four years after discharge may be warranted for children hospitalized with bronchiolitis.

ABSTRACT

Introduction: Acute respiratory infections (ARI) represent a leading cause of hospitalization in early childhood and may increase the risk of subsequent wheezing/asthma. However, longitudinal evidence of this association among Chinese children remains limited.

Methods: A follow-up cohort was established using the Yichang Health Management Big Data Platform, including children born between January 1, 2017, and December 31, 2018, who were hospitalized for ARI. Kaplan–Meier curves were used to estimate the cumulative incidence of subsequent wheezing/asthma, with group differences evaluated using the log-rank test. Piecewise Cox proportional hazards regression models were employed to assess the magnitude and timing of risk by ARI type.

Results: Among 22,460 children followed up for a median of 43.5 months, 1,463 developed wheezing/asthma. Hospitalization for bronchiolitis or pneumonia was associated with a significantly higher risk of wheezing/asthma than that for upper respiratory infection or influenza (P<0.001), with excess risk concentrated in the first 2 years. During the 2 to <4 years period, only bronchiolitis remained significantly associated with subsequent wheezing/asthma [adjusted hazard ratio (*aHR*)=1.85, 95% confidence interval (*CI*): 1.32, 2.58].

Conclusion: Children hospitalized for bronchiolitis or pneumonia experienced increased subsequent wheezing/asthma, particularly within 2 years of discharge. Structured follow-up and symptom-based asthma screening after discharge are essential, particularly in children with bronchiolitis.

Asthma is among the most prevalent chronic respiratory diseases in children, and acute respiratory infections (ARIs) represent a leading cause of hospitalization in early life (*1*). Severe respiratory infections in early childhood may increase the risk of subsequent wheezing and asthma; however, longitudinal evidence from Chinese pediatric populations remains scarce. Moreover, the magnitude and duration of this risk vary according to the infection type and follow-up period (*2*). Using the Yichang Health Management Big Data Platform, we established a follow-up cohort involving children born between January 1, 2017, and December 31, 2018, who were hospitalized for ARI. This birth period was selected to ensure a sufficient follow-up duration for assessing

subsequent wheezing/asthma outcomes during early childhood, while maintaining the completeness and consistency of longitudinal healthcare records through December 31, 2024. We examined the epidemiological features and temporal patterns of subsequent wheezing/asthma, focusing on variations in risk according to the infection type and follow-up period.

The Yichang Health Management Big Data Platform covers all 13 counties/districts in Yichang, comprising approximately 4.1 million residents. This platform integrates electronic medical records, and healthcare service data from medical institutions across the city, including outpatient and inpatient records. It is routinely maintained through data integration, quality control, and source data verification procedures. Following the removal of personal identifiers, hospitalization records were extracted for children born between January 1, 2017 and December 31, 2018, who were hospitalized for ARIs between January 1, 2017 and December 31, 2024, as identified using the International Classification of Diseases, 10th Revision (ICD-10) codes (J00–J06, J10–J11, J12–J18, J20, and J21). A unique identifier was assigned to each child to link records across institutions and time points, thereby enabling longitudinal follow-up. The first ARI hospitalization was defined as an index event. Repeat hospitalizations occurring within 28 days were considered part of the same infection episode. A 28-day washout period was applied following the index event to reduce the likelihood that wheezing/asthma diagnoses shortly after hospitalization reflected symptoms related to the acute infection episode rather than newly developed disease, consistent with previous epidemiological studies (*3*–*4*). The outcome was defined as a subsequent diagnosis of wheezing or asthma (ICD-10: R06.2, J45, and J46) identified from outpatient and inpatient records after the washout period. Follow-up began on day 29 post discharge and continued until the first outcome event or December 31, 2024, whichever occurred first. Supplementary Table S1(available at https://weekly.chinacdc.cn/) provides the specific ICD-10 codes for all diagnoses. The participant selection flowchart is shown in Supplementary Figure S1 (available at https://weekly.chinacdc.cn/). This study was exempted from ethical review as it utilized previously collected data that contained no personally identifiable information.

Continuous variables with normal distributions were summarized as means and standard deviations, whereas non-normally distributed variables were reported as medians and interquartile ranges (IQRs). Categorical variables were presented as frequencies and percentages. Sex differences were compared using the chi-square test, and linear trends across ordered age groups were evaluated using the Cochran-Armitage trend test. Kaplan–Meier analysis was employed to estimate the cumulative incidence of subsequent wheezing or asthma, with between-group differences assessed using the log-rank test. As Schoenfeld residual testing indicated that the proportional hazards assumption was violated for infection type (P<0.001), piecewise Cox proportional hazards regression models were fitted across three follow-up intervals: 0 to <2 years, 2 to <4 years, and 4 to <8 years (*5*). Adjusted hazard ratios (a*HR*s) and 95% confidence intervals (*CI*s) were calculated for each stratum. All analyses were conducted using R software (version 4.5.0; R Foundation for Statistical Computing, Vienna, Austria).

As shown in Table 1, 22,460 children hospitalized for acute respiratory infections were included in the analysis, of whom 1,463 developed wheezing or asthma during follow-up. The median follow-up duration was 43.50 months (IQR: 17.25–71.16). Pneumonia was the most prevalent infection type (50.65%), followed by upper respiratory tract infections (26.71%) and bronchitis (15.31%). The distribution of infection types differed significantly between children who did and did not develop subsequent wheezing or asthma (P<0.001). Children who developed wheezing or asthma were more likely to be male (61.79% *vs*. 53.14%, P<0.001) and younger at the time of ARI hospitalization (median: 1.36 years *vs*. 3.17 years, P<0.001). The proportion of children aged 0 to <2 years was higher in the wheezing or asthma group, whereas the proportion aged 5 to <8 years was lower (P<0.001). Calendar period of the index ARI hospitalization differed significantly by subsequent asthma status (χ^2=457.06, P<0.001), with a higher proportion of children with subsequent wheezing or asthma hospitalized during 2017–2019 and a lower proportion during 2023–2024.

Kaplan–Meier curves revealed significant differences in cumulative wheezing/asthma incidence across infection types (log-rank P<0.001) (Figure 1). Bronchiolitis exhibited the highest cumulative incidence, followed by pneumonia, whereas upper respiratory tract infections and influenza were associated with lower cumulative incidences.

Kaplan–Meier curves showed significant differences in the cumulative wheezing/asthma incidence across infection types. Given that the proportional hazards

TABLE 1. Baseline characteristics of children hospitalized for acute respiratory infections by subsequent wheezing/asthma status, 2017–2024.

Characteristics	Total (*n*=22,460)	Without subsequent wheezing/asthma (*n*=20,997)	With subsequent wheezing/asthma (*n*=1,463)	Statistic	*P*
Infection type				100.77	<0.001
URTI	6,000 (26.71)	5,685 (27.08)	315 (21.53)		
Influenza	715 (3.18)	691 (3.29)	24 (1.64)		
Pneumonia	11,375 (50.65)	10,565 (50.32)	810 (55.37)		
Bronchitis	3,439 (15.31)	3,245 (15.45)	194 (13.26)		
Bronchiolitis	931 (4.15)	811 (3.86)	120 (8.20)		
Sex				40.81	<0.001
Male	12,062 (53.70)	11,158 (53.14)	904 (61.79)		
Female	10,398 (46.30)	9,839 (46.86)	559 (38.21)		
Birth year				1.78	0.183
2017	11,497 (51.19)	10,723 (51.07)	774 (52.90)		
2018	10,963 (48.81)	10,274 (48.93)	689 (47.10)		
Birth season				5.62	0.132
Spring	5,219 (23.24)	4,896 (23.32)	323 (22.08)		
Summer	5,660 (25.20)	5,310 (25.29)	350 (23.92)		
Autumn	5,795 (25.80)	5,418 (25.80)	377 (25.77)		
Winter	5,786 (25.76)	5,373 (25.59)	413 (28.23)		
Age at first ARI hospitalization, years	2.91 (0.85, 5.18)	3.18 (0.87, 5.30)	1.37 (0.69, 2.85)	–	<0.001
Age group at first ARI hospitalization, years				418.19	<0.001
0–1	9,801 (43.64)	8,866 (42.23)	935 (63.91)		
2–4	6,504 (28.96)	6,048 (28.80)	456 (31.17)		
5–7	6,155 (27.40)	6,083 (28.97)	72 (4.92)		
Calendar period of the index ARI hospitalization				457.06	<0.001
2017–2019	10,085 (44.90)	9,102 (43.35)	983 (67.19)		
2020–2022	6,008 (26.75)	5,611 (26.72)	397 (27.14)		
2023–2024	6,367 (28.35)	6,284 (29.93)	83 (5.67)		

Note: "–" means not applicable. Categorical variables were presented as *n* (%), and age at ARI hospitalization is presented as median (Q1, Q3). Between-group comparisons for infection type, sex, birth year, birth season, and calendar period of ARI hospitalization were performed using the chi-square test; the comparison of age at ARI hospitalization was compared using the Wilcoxon rank-sum test; and the linear trend across ordered age groups was assessed using the Cochran–Armitage trend test.
Abbreviation: ARI=acute respiratory infection; URTI=upper respiratory tract infection.

assumption was violated for infection type, piecewise Cox proportional hazards regression models were applied. As presented in Table 2 and Supplementary Figure S2 (available at https://weekly.chinacdc.cn/), bronchiolitis and pneumonia were associated with increased wheezing or asthma risk during 0 to <2 years after hospitalization [a*HR*=3.42 (95% *CI*: 2.48, 4.71) and 2.15 (95% *CI*: 1.75, 2.65), respectively], and bronchiolitis remained associated during 2 to <4 years [a*HR*=1.85 (95% *CI*: 1.32, 2.58)]. No significant associations were observed between ages 4 and 8 years.

DISCUSSION

This study found that children hospitalized for bronchiolitis or pneumonia had a substantially higher subsequent risk of wheezing/asthma than those hospitalized for upper respiratory tract infection or influenza. The excess risk was concentrated primarily within the first two years following hospitalization and gradually attenuated thereafter. Beyond 2 years, only bronchiolitis remained significantly associated with an elevated risk during the 2 to 4 years period, and no significant differences by infection type were detected

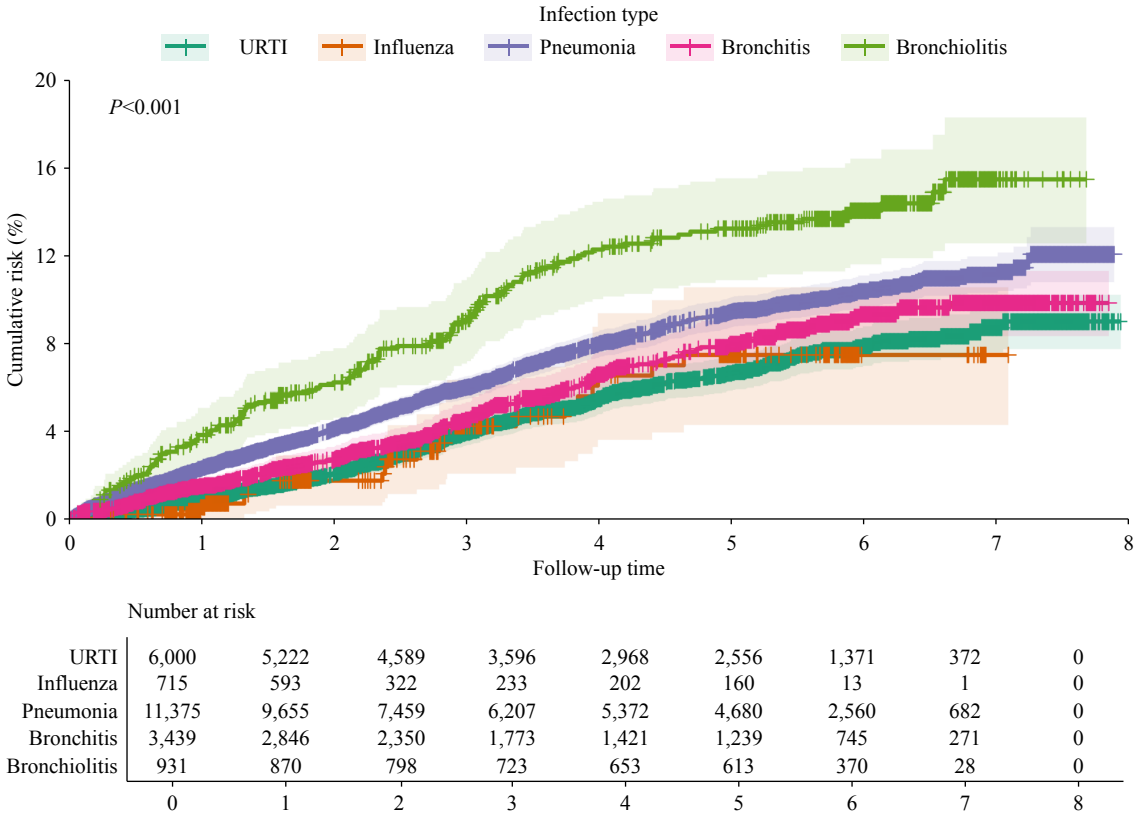

FIGURE 1. Cumulative risk of wheezing/asthma among children hospitalized for different types of acute respiratory infections, Yichang City, Hubei Province, China, 2017–2024.
Abbreviation: ARI=acute respiratory infection; URTI=upper respiratory tract infection.

TABLE 2. Piecewise Cox proportional hazards regression analyses of subsequent wheezing/asthma among children hospitalized for acute respiratory infections, Yichang City, Hubei Province, China, 2017–2024.

Variables	0 to <2 years a*HR* (95% *CI*)	2 to <4 years a*HR* (95% *CI*)	4 to <8 years a*HR* (95% *CI*)
URTI	1.00 (Ref)	1.00 (Ref)	1.00 (Ref)
Influenza	0.89 (0.47, 1.71)	1.34 (0.74, 2.42)	0.54 (0.13, 2.19)
Pneumonia	2.15 (1.75, 2.65)***	1.16 (0.94, 1.43)	1.07 (0.80, 1.42)
Bronchitis	1.33 (1.00, 1.76)*	1.15 (0.86, 1.53)	1.08 (0.73, 1.61)
Bronchiolitis	3.42 (2.48, 4.71)***	1.85 (1.32, 2.58)***	0.89 (0.51, 1.56)

Note: Hazard ratios were adjusted for sex, birth year, birth season, age at first ARI hospitalization, and the calendar period of the index ARI hospitalization. URTI was used as the reference group.
Abbreviation: a*HR*=adjusted hazard ratio; *CI*=confidence interval; Ref=reference; ARI=acute respiratory infection; URTI=upper respiratory tract infection.
* *P*<0.1; *** *P*<0.001.

after 4 years.

These findings are broadly consistent with those in the existing literature. Similarly, a recent single-center long-term follow-up study in China reported that children hospitalized for bronchiolitis in early life had an elevated risk of recurrent wheezing (*6*). A population-based cohort study from Spain demonstrated that early-life bronchiolitis was associated with an increased risk of recurrent wheezing and asthma and that this association was not fully explained by pathogen type or disease severity (*7*). In contrast, a smaller longitudinal study conducted in the United Kingdom did not identify a clear direct association between early lower respiratory tract infections and subsequent asthma outcomes (*8*). This discrepancy may reflect the small sample size, short follow-up duration, and differences in infection severity across the study populations.

Notably, the risk of subsequent wheezing/asthma following ARI hospitalization was concentrated

predominantly within the first 2 years and gradually diminished thereafter. Only bronchiolitis maintained a significant association with increased risk during the 2 to <4 year interval, and no infection type differences persisted beyond 4 years, further underscoring the distinctive link between bronchiolitis and the development of asthma. This temporal pattern aligns with findings from a Scottish cohort study demonstrating that severe RSV-related respiratory infections confer the greatest asthma risk within the first 2 years after infection (*4*). Accordingly, our results suggest that the first 2 years post-discharge represent a critical follow-up window, with extended monitoring warranted for children hospitalized with bronchiolitis. Some prior studies have reported that the association between early respiratory infections and asthma may persist up to the age of 10 years. The attenuated late effect observed in our study may reflect differences in regional healthcare data systems and diagnostic or healthcare-seeking behaviors. Additionally, as children age, the growing influence of unmeasured host and environmental factors on wheezing/asthma risk may progressively dilute the contribution of early-life infections (*9*).

One possible explanation for this association is that lower respiratory tract infections, particularly bronchiolitis and pneumonia, involve the small airways and lung parenchyma more extensively than upper respiratory tract infections or influenza, which may be markers of greater airway vulnerability, more intense inflammatory responses, or underlying host susceptibility to recurrent wheezing and asthma (*6*). In addition, infections occurring during early life may coincide with critical periods of immune and pulmonary development, which may help explain the stronger association observed within the first two years after hospitalization (*9*–*10*). However, given the observational design and the absence of detailed data on host, environmental, and immunological factors, these findings should not be interpreted as evidence of a direct causal pathway.

This study had several notable strengths. First, it leveraged real-world medical data with longitudinal linkage across healthcare institutions, yielding a large population-based sample for evaluating long-term outcomes following ARI hospitalization. Second, the application of piecewise Cox proportional hazards regression enabled the capture of temporal variations in wheezing and asthma risk, facilitating the identification of the first two years as a critical follow-up window. Nevertheless, this study had several limitations that warrant consideration. First, ARI exposure and outcomes were ascertained using ICD-10 codes, which may have introduced coding errors or diagnostic misclassifications. Second, residual confounding from unmeasured factors, including socioeconomic status, family history of atopy, prematurity, and environmental tobacco smoke exposure, cannot be ruled out and might lead to overestimation of the associations. Therefore, our findings should be interpreted as associations rather than definitive causal effects. Future studies should incorporate these variables to delineate the determinants of post-ARI wheezing and asthma more precisely. Finally, the coronavirus disease 2019 (COVID-19) pandemic may have influenced the overall background pattern of ARI hospitalizations during the study period. However, the calendar period analyses suggested that the main associations of interest did not materially change. Because this cohort was derived from a single city and spanned the pandemic period, caution is warranted when generalizing the findings to other regions or pre- or post-pandemic settings.

In conclusion, hospitalization for bronchiolitis or pneumonia was associated with an increased subsequent risk of wheezing or asthma, with the excess risk concentrated primarily within the first two years after hospitalization. These findings support structured respiratory follow-up and symptom-based asthma screening for children hospitalized with bronchiolitis or pneumonia during the first two years after discharge. For children hospitalized with bronchiolitis, an extended follow-up of 4 years after discharge may be warranted. Future studies across diverse regions and cohorts, incorporating more detailed clinical and environmental exposure data, are warranted to strengthen the evidence base for respiratory health management following ARI hospitalization.

Conflicts of interest: No conflicts of interest.

doi: 10.46234/ccdcw2026.104

[#] Corresponding authors: Jinfang Sun, sunjf@chinacdc.cn; Guoxing Li, liguoxing@bjmu.edu.cn.

[1] Office of Epidemiology (Technical Guidance Office for Patriotic Health Work), Chinese Center for Disease Control and Prevention & Chinese Academy of Preventive Medicine, Beijing, China; [2] Infectious Disease Prevention, Control and Supervision Institute of Yichang Center for Disease Control and Prevention, Yichang, Hubei Province, China; [3] School of Public Health, Peking University Health Science Center, Beijing, China.

Submitted: March 19, 2026
Accepted: May 14, 2026
Issued: May 22, 2026

REFERENCES

1. van Meel ER, Mensink-Bout SM, den Dekker HT, Ahluwalia TS, Annesi-Maesano I, Arshad SH, et al. Early-life respiratory tract infections and the risk of school-age lower lung function and asthma: A meta-analysis of 150 000 European children. Eur Respir J 2022;60(4): 2102395. https://doi.org/10.1183/13993003.02395-2021.
2. Shiroshita A, Gebretsadik T, Wu PS, Kubilay NZ, Hartert TV. Association between age of respiratory syncytial virus infection hospitalization and childhood asthma: A systematic review. PLoS One 2024;19(2):e0296685. https://doi.org/10.1371/journal.pone.0296685.
3. Hu YZ, Yu CQ, Guo Y, Bian Z, Han YT, Yang L, et al. Pneumonia hospitalizations and the subsequent risk of incident ischaemic cardiovascular disease in Chinese adults. Int J Epidemiol 2021;50(5): 1698 – 707. https://doi.org/10.1093/ije/dyab039.
4. Wang X, Li Y, Nair H, Campbell H, RESCEU Investigators. Time-varying association between severe respiratory syncytial virus infections and subsequent severe asthma and wheeze and influences of age at the infection. J Infect Dis 2022;226(S1):S38 – 44. https://doi.org/10.1093/infdis/jiab308.
5. Zhang ZH, Reinikainen J, Adeleke KA, Pieterse ME, Groothuis-Oudshoorn CGM. Time-varying covariates and coefficients in Cox regression models. Ann Transl Med 2018;6(7):121. https://doi.org/10.21037/atm.2018.02.12.
6. Chen SN, Xu XY, Wu M, Zhou LT, Wang YQ. Risk factors for recurrent wheezing after infant bronchiolitis: A 6-year single-centre follow up study in China. Front Pediatr 2025;13:1549475. https://doi.org/10.3389/fped.2025.1549475.
7. Muñoz-Quiles C, López-Lacort M, Díez-Domingo J, Orrico-Sánchez A. Bronchiolitis, regardless of its etiology and severity, is associated with increased risk of asthma: A population-based study. J Infect Dis 2023;228(7):840 – 50. https://doi.org/10.1093/infdis/jiad093.
8. Ramette A, Spycher BD, Wang JY, Goutaki M, Beardsmore CS, Kuehni CE. Longitudinal associations between respiratory infections and asthma in young children. Am J Epidemiol 2018;187(8):1714 – 20. https://doi.org/10.1093/aje/kwy053.
9. van Meel ER, den Dekker HT, Elbert NJ, Jansen PW, Moll HA, Reiss IK, et al. A population-based prospective cohort study examining the influence of early-life respiratory tract infections on school-age lung function and asthma. Thorax 2018;73(2):167 – 73. https://doi.org/10.1136/thoraxjnl-2017-210149.
10. Lloyd CM, Saglani S. Early-life respiratory infections and developmental immunity determine lifelong lung health. Nat Immunol 2023;24(8):1234 – 43. https://doi.org/10.1038/s41590-023-01550-w.

SUPPLEMENTARY MATERIALS

SUPPLEMENTARY TABLE S1. Detailed listing of ICD-10 codes for diseases.

Categories	Subcategories of diseases and corresponding ICD-10 codes
Acute upper respiratory infections	Acute nasopharyngitis [common cold] (J00); Acute sinusitis (J01); Acute pharyngitis (J02); Acute tonsillitis (J03); Acute laryngitis and tracheitis (J04); Acute obstructive laryngitis [croup] and epiglottitis (J05); Acute upper respiratory infections of multiple and unspecified sites (J06)
Influenza	Influenza due to identified influenza virus (J10); Influenza, virus not identified (J11)
Pneumonia	Viral pneumonia, not elsewhere classified (J12), Pneumonia due to *Streptococcus* (J13), Pneumonia due to Haemophilus influenzae (J14), Bacterial pneumonia, not elsewhere classified (J15), Pneumonia due to other infectious organisms, not elsewhere classified (J16), Pneumonia in diseases classified elsewhere (J17), Pneumonia, organism unspecified (J18)
Bronchitis	Acute bronchitis (J20)
Bronchiolitis	Acute bronchiolitis (J21)
Wheezing	Wheezing (R06.2)
Asthma	Asthma (J45), Status asthmaticus (J46)

Abbreviation: ICD-10=International Classification of Diseases, 10th Revision; ARI=acute respiratory infection.

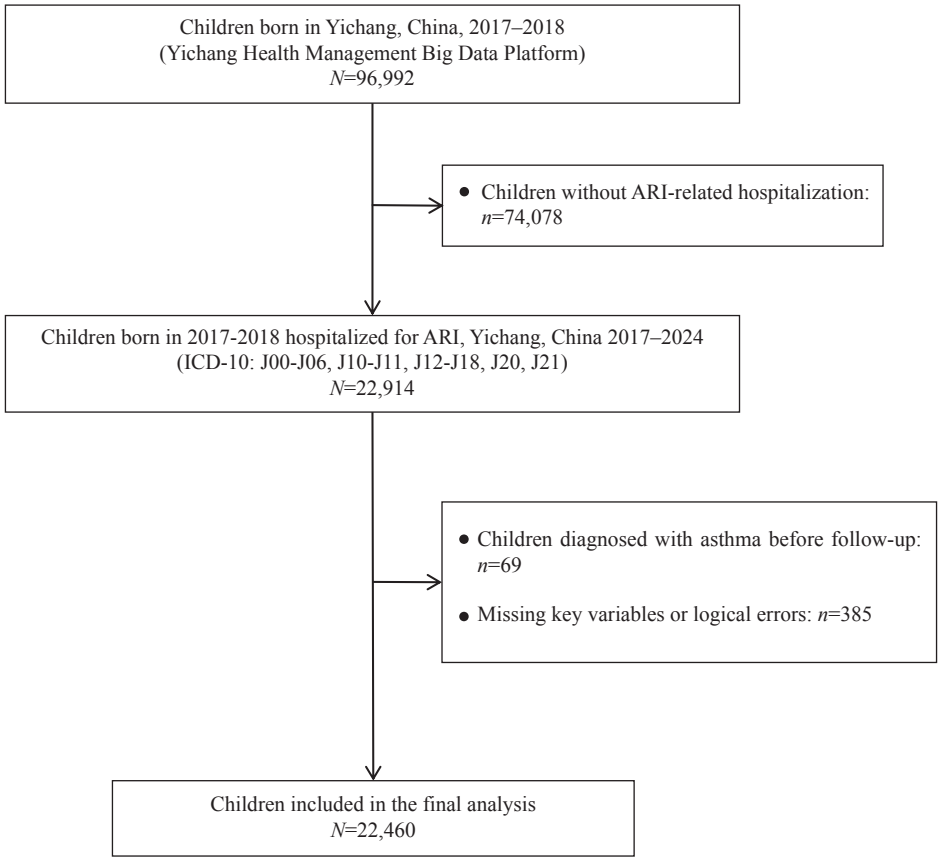

SUPPLEMENTARY FIGURE S1. Flow chart of study participant selection.
Abbreviation: ARI=acute respiratory infection.

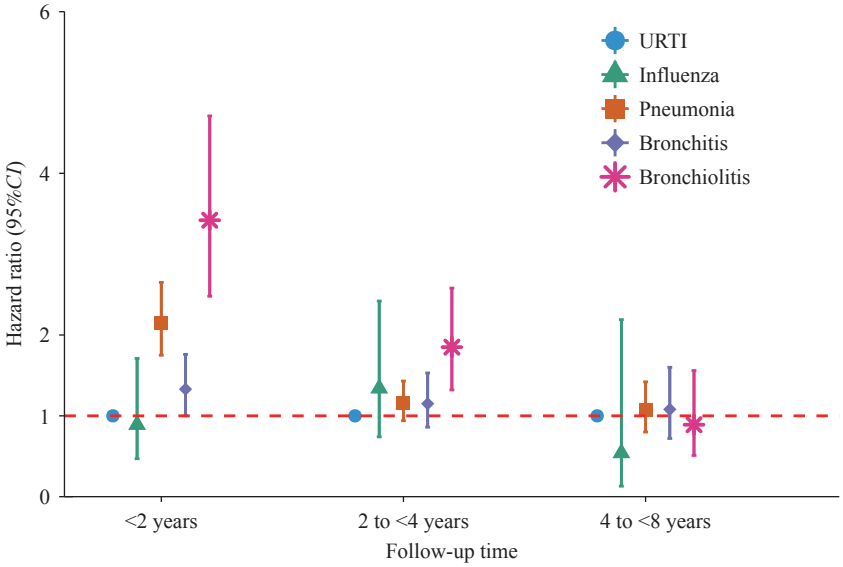

SUPPLEMENTARY FIGURE S2. Forest plot for subsequent wheezing or asthma among children hospitalized for acute respiratory infections in Yichang City, Hubei Province, China, 2017–2024.
Abbreviation: a*HR*=adjusted hazard ratio; *CI*=confidence interval; Ref=reference.

Preplanned Studies

Analysis of Spatiotemporal Variation Characteristics and Influencing Factors of Human Brucellosis — Shaanxi Province, China, 2015–2024

Ying Li[1]; Jiarui Yuan[1]; Zhe Li[1]; Shoumin Nie[1]; Boyan Luo[1]; Dijia Zhou[1]; Wenjing Wang[1]; Yangxin Sun[1]; Cuihong An[1]; Suoping Fan[1]; Zhaoxing Lin[1]; Yongbing Cheng[1,#]

Summary

What is already known about this topic?

Human brucellosis poses a serious threat to the health of residents in Shaanxi Province, China.

What is added by this report?

Between 2015 and 2024, the annual incidence rate of human brucellosis in Shaanxi, China, remained at historically high levels, exhibiting a high-to-low gradient from north to south, and its influencing factors demonstrated spatiotemporal heterogeneity.

What are the implications for public health practice?

Targeted surveillance and control strategies for human brucellosis should be implemented according to local epidemiological characteristics. Surveillance and early warning capacity in the high-risk areas must be strengthened, and differentiated prevention and control measures should be developed accordingly.

ABSTRACT

Introduction: Human brucellosis poses a significant threat to public health in Shaanxi Province, China. Understanding the long-term epidemiological trends is essential for developing targeted prevention and control strategies.

Methods: Based on human brucellosis surveillance data from Shaanxi from 2015 to 2024, a seasonal autoregressive integrated moving average and extreme gradient boosting (SARIMA-XGBoost) time-series model was constructed and spatial autocorrelation analysis was performed to characterize temporal trends and spatial clustering. Geographically and temporally weighted regression (GTWR) was applied to identify factors associated with spatiotemporal heterogeneity in disease distribution. Before GTWR modeling, a geodetector and collinearity diagnostics were used for variable selection.

Results: Human brucellosis cases were reported between 2015 and 2024 in all the prefectural cities in Shaanxi. Monthly incidence rates ranged from 0.02 to 0.61 per 100,000 population. Temporally, the incidence showed seasonal distribution. SARIMA-XGBoost predicted that the incidence rate in 2025 would first increase and then decrease. Spatially, the incidence rate of human brucellosis in Shaanxi demonstrated annual clustering and a high-to-low gradient from northern to southern prefectural cities. The GTWR indicated that the spatiotemporal distribution of human brucellosis was associated with inventories of cattle, buffalo, sheep, goats, and meteorological factors.

Conclusion: The human brucellosis epidemic in Shaanxi exhibited distinct spatiotemporal transmission patterns. SARIMA-XGBoost effectively captured its temporal trends, while the spatiotemporal heterogeneity of livestock inventory and meteorological factors provide an important basis for targeted prevention and control strategies.

Brucellosis is a zoonotic disease caused by infection with *Brucella* bacteria. Human brucellosis infection occurs mainly through direct contact with infected livestock materials or consumption of unpasteurized dairy products and undercooked animal products. According to the WHO, over 500,000 people worldwide contract brucellosis annually. In China, brucellosis is classified as a Category B notifiable infectious disease, and Northwest China remains a high-prevalence region for this pathogen (*1*). As China's "dual milk source" base for both dairy goats and dairy cows, Shaanxi has successively established demonstration zones, such as brucellosis-free zones for cattle, sheep, and goats, and brucellosis eradication zones for dairy goats, which have effectively controlled

the local epidemic (*2*). However, the optimization and upgrading of Shaanxi's livestock industry chain have created new challenges for human brucellosis prevention and control. Therefore, this study aims to investigate the long-term trends and influencing factors of human brucellosis in Shaanxi from 2015 to 2024.

This study used monthly human brucellosis incidence data for prefecture-level cities in Shaanxi (2015–2024) from China's infectious disease surveillance subsystem and collected annual data on livestock, meteorological conditions, and healthcare resources from the Shaanxi Provincial Statistical Yearbook.

First, we constructed a time-series model based on Seasonal Autoregressive Integrated Moving Average and Extreme Gradient Boosting (SARIMA-XGBoost) for the monthly incidence of human brucellosis in Shaanxi (2015–2024) using the R software (version 4.3.1; R Foundation for Statistical Computing, Vienna, Austria). The dataset was divided into training and validation sets at a ratio of 8∶2. Optimal SARIMA parameters were selected using auto_arima, and residuals from the SARIMA model were fed into a sliding-window XGBoost model with grid search to minimize the average root mean square error (RMSE) and construct the combined prediction model (Supplementary Table S1, available at https://weekly.chinacdc.cn/). Model performance was evaluated using residuals, RMSE, mean absolute error (MAE), and mean absolute percentage error (MAPE). The model was then used to predict monthly incidence in 2025. Second, a k-nearest neighbor spatial weight matrix (k=3) was constructed, and Global and Local Moran's I values were calculated to assess spatial clustering. Third, data from 2015–2024 on livestock inventory (cattle/buffaloes and sheep/goats), meteorological factors, and healthcare resources were standardized using Z-score normalization. Geodetector analysis and collinearity diagnostics were used to identify factors with high explanatory power and no multicollinearity (Supplementary Table S2, available at https://weekly.chinacdc.cn/). Subsequently, using annual incidence data for 2015–2024 across 10 prefectural cities and year as the temporal dimension, a geographically and temporally weighted regression (GTWR) model was fitted through spatiotemporal distance weighting with adaptive bandwidths to minimize the corrected Akaike information criterion (AICc). Model fit was assessed using adjusted R^2, AICc, and residual sum of squares (RSS), and factor coefficients were calculated to interpret spatiotemporal heterogeneity.

From January 2015 to December 2024, the monthly brucellosis incidence in Shaanxi ranged from 0.02–0.61 per 100,000 population, with a mean of 0.26 per 100,000 population. Cases were reported in all prefectural cities, with Yulin accounting for the highest proportion (Supplementary Figure S1, available at https://weekly.chinacdc.cn/). The SARIMA-XGBoost model outperformed standalone SARIMA across all metrics (Supplementary Table S3, available at https://weekly.chinacdc.cn/). The combined model predicted that monthly incidence in 2025 would first increase and then decrease, with cases concentrated between April and August (Figure 1), which closely matched the observed trends, with an average deviation of 7.17%.

Global clustering analysis revealed annual spatial aggregation of human brucellosis in Shaanxi, although the duration varied. Clustering occurred only in certain months during 2017–2020 but was present year-round in other years. All Global Moran's I values for clustered months were positive, indicating significant positive spatial autocorrelation in human brucellosis incidence across Shaanxi (Figure 2). Local clustering analysis showed that clustering patterns remained stable across regions: Northern Shaanxi presented high–high clusters, Southern Shaanxi showed low–low clusters, and Central Shaanxi exhibited a random distribution (Supplementary Figure S2, available at https://weekly.chinacdc.cn/).

Model fitting showed that GTWR outperformed ordinary least squares (OLS) regression (Supplementary Table S4, available at https://weekly.chinacdc.cn/), indicating potential heterogeneity in the magnitude and direction of associations between influencing factors and brucellosis incidence in Shaanxi (Table 1). Among the factors, the estimated coefficients for sheep and goat inventory were >0 across years and regions, indicating a positive association on brucellosis incidence, with the effect intensity showing a pattern of "highest in central Shaanxi and lowest in northern Shaanxi." The estimated coefficients for cattle and buffalo inventory and average wind speed were both <0, indicating negative associations, with the spatial distribution of intensity being "highest for cattle and buffaloes in central Shaanxi and highest for wind speed in northern Shaanxi." The maximum and minimum estimated coefficients had opposite signs for the average temperature, relative humidity, and precipitation, indicating bidirectional effects that varied in intensity across regions (Table 2).

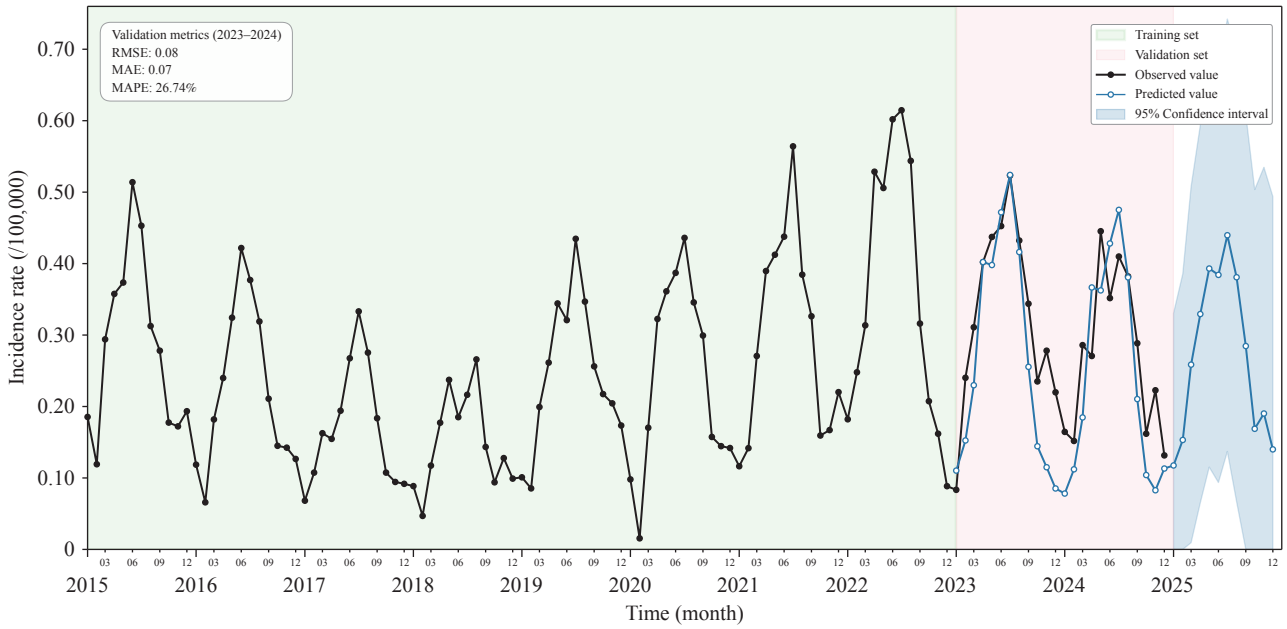

FIGURE 1. Distribution of brucellosis incidence rate and SARIMA-XGBoost projections in Shaanxi Province, 2015–2025.
Note: The 95% confidence interval was constructed by adding the 95% prediction interval of SARIMA and the 95% interval of the XGBoost-predicted residuals.
Abbreviation: RMSE=root mean square error; MAE=mean absolute error; MAPE=mean absolute percentage error.

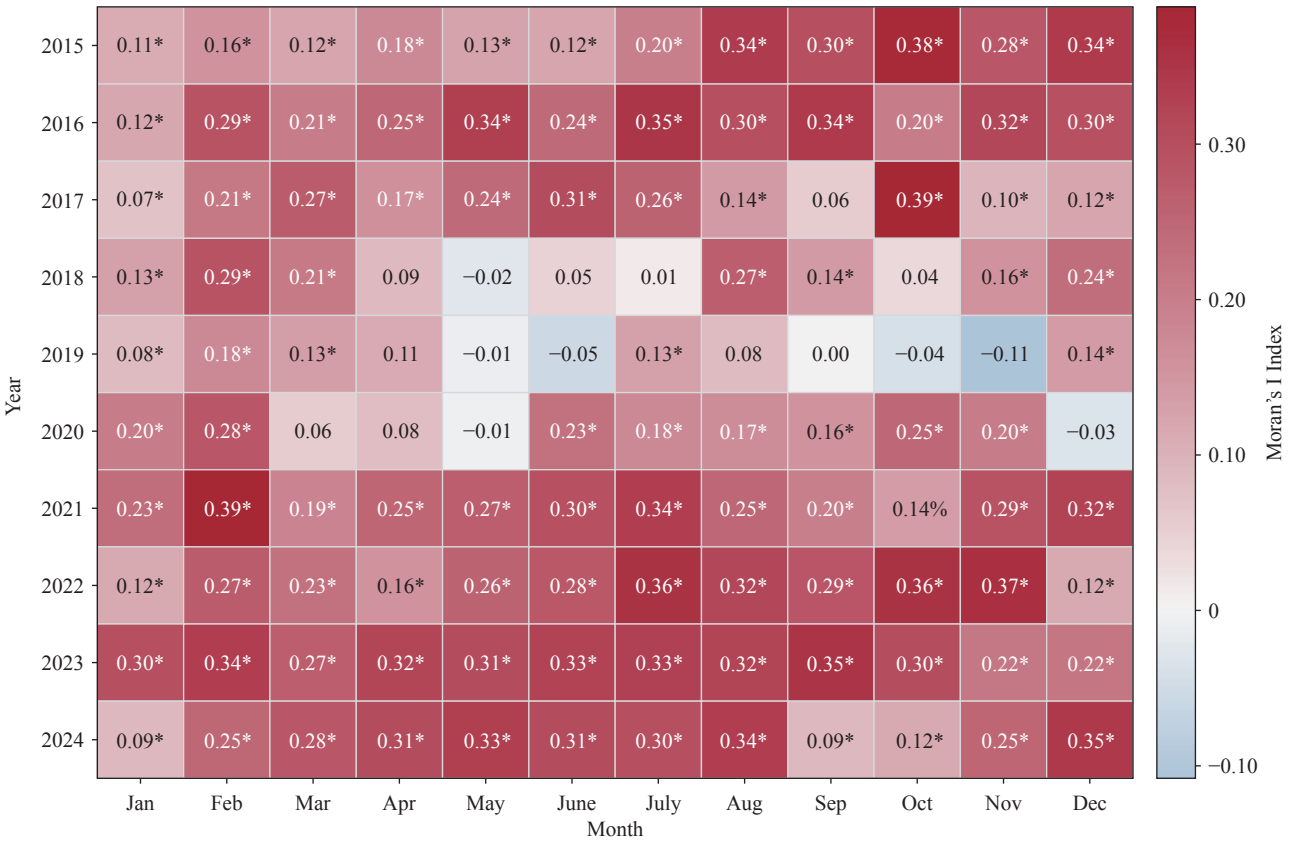

FIGURE 2. Heatmap of monthly global spatial clustering results for brucellosis in Shaanxi Province, 2015–2024.
* indicates statistical significance ($P \leq 0.05$).

TABLE 1. Statistical distribution of GTWR and OLS estimation results for brucellosis in Shaanxi Province.

Influencing factors	GTWR					OLS	
	Minimum	1st Quarter	Median	3rd Quarter	Maximum	Estimate	*P*
Intercept	−4.63	12.9	18.82	23.11	34.26	21.97	<0.01
Sheep and goat inventory (10,000 head)	0.16	0.17	0.23	0.38	0.68	0.17	<0.01
Cattle and buffalo inventory (10,000 head)	−1.57	−0.87	−0.57	−0.55	−0.40	−0.50	0.10
Average temperature (℃)	−1.04	−0.87	−0.59	−0.38	0.08	−0.90	<0.01
Relative humidity (%)	−0.15	−0.08	−0.04	−0.01	0.18	−0.03	0.70
Average wind speed (m/s)	−3.37	−2.00	−1.76	−1.21	−0.13	−1.61	0.08
Precipitation (100 mm)	−0.82	−0.30	−0.31	−0.10	0.06	−0.32	0.04

Note: Descriptive statistics were calculated from 100 spatiotemporally varying local coefficient estimates generated by GTWR.
Abbreviation: GTWR=geographically and temporally weighted regression; OLS=ordinary least squares.

TABLE 2. Spatial distribution of median coefficients of influencing factors for brucellosis in Shaanxi Province.

Cities	Sheep and goat inventory (10,000 head)	Cattle and buffalo inventory (10,000 head)	Average temperature (℃)	Relative humidity (%)	Average wind speed (m/s)	Precipitation (100 mm)
Yulin	0.17	−0.53	−0.82	−0.01	−2.03	−0.47
Yan'an	0.17	−0.52	−0.82	−0.03	−2.34	−0.50
Tongchuan	0.37	−1.05	−0.26	0.01	−1.80	−0.24
Xianyang	0.41	−1.11	−0.26	0	−1.72	−0.24
Weinan	0.33	−0.86	−0.36	−0.04	−1.80	−0.25
Xi'an	0.37	−1.06	−0.30	0.00	−1.75	−0.24
Baoji	0.31	−0.81	−0.42	−0.05	−1.33	−0.25
Shangluo	0.27	−0.58	−0.61	−0.10	−1.69	−0.28
Hanzhong	0.23	−0.56	−0.56	−0.04	−1.14	−0.23
Ankang	0.23	−0.50	−0.61	−0.05	−1.29	−0.25

DISCUSSION

Currently, the incidence of human brucellosis in Shaanxi remains historically high, with pronounced seasonal clustering and widespread distribution across all 10 prefectural cities. This study explored its spatiotemporal patterns and driving factors using SARIMA-XGBoost and GTWR. The results revealed distinct spatiotemporal patterns: temporally, the incidence was concentrated in spring and summer, and spatially, the incidence decreased from northern to southern Shaanxi. This trend was likely associated with the intensity of livestock farming and meteorological conditions. These findings provide preliminary insights into factors influencing brucellosis and support the formulation of targeted regional prevention and control strategies in Shaanxi.

Shaanxi hosts the largest dairy goat base county in China, with an inventory of cattle, buffaloes, sheep, and goats reaching 10.69 million heads and milk production of up to 1.10 million tons. A large population engaged in related occupations faces a high risk of brucellosis infection (*3*). Studies have shown that the peak incidence of human brucellosis coincides with the peak breeding season for livestock (*4*). Winter and spring are the peak breeding seasons for cattle, buffalo, sheep, and goats in Shaanxi. During this period, livestock breeders face increased risk of infection through contact with infected animal placentas and aborted fetuses, and after the incubation period, cases are concentrated in spring and summer. The SARIMA-XGBoost not only captures the long-term trends and seasonal characteristics of brucellosis incidence but also accounts for the impact of recent events. The predicted results indicated that brucellosis in Shaanxi will continue to exhibit seasonal incidence in 2025, although the predicted values are slightly higher than the observed values. This may be attributed to the fact that Shaanxi has completely broken down the coordination barriers between animal husbandry and disease control systems and has

established a full-process linked to the prevention and control system (*5*).

Our study found that the brucellosis incidence in Shaanxi was positively correlated with the sheep and goat inventory, but negatively correlated with the cattle and buffalo inventory. These findings may reflect differences in livestock farming models, regional distribution of livestock, and the susceptibility of the human population to different *Brucella* strains (*6*). Shaanxi has a large inventory of sheep and goats. Numerous smallholder farmers are geographically concentrated in northern Shaanxi and generally have limited protective awareness, making them more vulnerable to *Brucella melitensis* (goat strain) infection. In comparison, cattle and buffalo breeding is dominated by standardized large-scale farms with a geographically balanced layout across northern, central, and southern Shaanxi. Such farms implement rigorous management protocols and occupational health protections for staff. Additionally, *Brucella abortus* (cattle strain) is less virulent in humans than the goat strain. Collectively, sheep and goat inventories may serve as core drivers of Shaanxi's brucellosis epidemics, while large-scale cattle and buffalo breeding may dilute the transmission risk. This inference is further supported by Shaanxi's north-high and south-low spatial clustering patterns of brucellosis.

As a zoonotic disease, meteorological factors affect the survival and transmission of *Brucella* in natural environments, and indirectly regulate human exposure risk by altering production and living behaviors (*7*). Our results showed that the average wind speed was negatively correlated with the incidence of brucellosis in Shaanxi, possibly because strong winds diluted aerosolized *Brucella* and reduced its environmental concentration. Additionally, the average temperature, relative humidity, and rainfall had heterogeneous effects, mostly negative but positive in some periods or regions, indicating bidirectional regulation. The optimal growth temperature for *Brucella* is 35°C–37 °C (*8*). Moderately high temperatures facilitate *Brucella* growth and reproduction in hosts, whereas extreme heat accelerates bacterial inactivation and reduces outdoor human exposure, thus lowering disease risk. Low humidity favors airborne *Brucella* transmission, which elevates the risk of human infection (*9*), whereas high humidity slows bacterial dehydration and prolongs pathogen survival in fur, soil, and livestock housing, thereby increasing the risk of contact infection. Moderate rainfall can enhance livestock immunity by promoting vegetation growth and suppressing the incidence of brucellosis, whereas heavy rainfall can contaminate water sources and pastures via surface runoff, increasing livestock exposure, aggravating cross-infection, and the risk of human infection.

This study had some limitations. First, the combined model used a rolling smoothing window; however, the window length was fixed. Future studies could further optimize the window length in light of pathogen evolution. Second, this study only covered incidence data from prefectural cities in Shaanxi over ten years, which, to some extent, limits the goodness-of-fit and generalizability of the model. Future research could refine the analysis unit to the monthly and county-levels. Third, this study only analyzed the contemporaneous effects of the influencing factors and did not explore their lagged effects on brucellosis incidence. However, the underlying mechanism warrants further investigation.

In summary, the human brucellosis epidemic in Shaanxi has exhibited spatiotemporal transmission patterns. SARIMA-XGBoost can effectively capture the temporal trends of brucellosis incidence and improve the prediction accuracy and stability. The spatiotemporal heterogeneity of livestock inventory and meteorological factors suggests that the driving mechanisms of epidemics may differ across regions. Accordingly, the prevention and control of brucellosis in Shaanxi should focus on source control. Priority should be given to infection prevention and control among smallholder farmers and the promotion of large-scale, standardized farming models. Simultaneously, it is essential to align the high incidence pattern in spring and summer to strengthen seasonal surveillance and early warning. The findings of this study may support targeted brucellosis prevention strategy formulation in Shaanxi and offer a reference for the control of other natural focal diseases.

Conflicts of interest: No conflicts of interest.

doi: 10.46234/ccdcw2026.105

[#] Corresponding author: Yongbing Cheng, sxcdc@sxcdc.com.

[1] Shaanxi Provincial Center for Disease Control and Prevention, Xi'an City, Shaanxi Province, China.

Submitted: March 09, 2026
Accepted: May 15, 2026
Issued: May 22, 2026

REFERENCES

1. Zhao Y, Pan DF, Zhang YF, Ma LX, Li H, Li JJ, et al. Spatial interpolation and spatiotemporal scanning analysis of human brucellosis in mainland China from 2012 to 2018. Sci Rep 2025;15(1):7403. https://doi.org/10.1038/s41598-025-91769-4.
2. Zhu WY, Zhao YP, Xie YQ, Dai DH, Pan KS, Ye DY. Prevention and control strategies for brucellosis of dairy goats in Guanzhong area of Shaanxi province: an exploration. Feed Rev 2024(3):27 – 30. https://doi.org/10.20041/j.cnki.slbl.2024.03.006.
3. Shaanxi Provincial Bureau of Statistics, Shaanxi Survey Team of National Bureau of Statistics. Shaanxi statistical yearbook 2024. Beijing: China Statistics Press. 2024. https://book.kongfz.com/26152/7787891185. (In Chinese).
4. Chen YC, Yang SH, Hua J, Pan LY, Ji CL, Zhang Z, et al. Analysis on epidemiological characteristics of human brucellosis and influencing factors of delayed diagnosis in Dalian of Liaoning, 2006-2022. Dis Surveill 2024;39(8):995 – 1000. https://doi.org/10.3784/jbjc.202308160421.
5. Shaanxi Provincial Department of Agriculture and Rural Affairs. Shaanxi Provincial Animal Health and Slaughter Management Station signs brucellosis joint prevention and control agreement with Shaanxi Provincial Center for Disease Control and Prevention. 2025. http://nynct.shaanxi.gov.cn/sy/sbxx/202506/t20250627_3536749.html. [2026-4-27]. (In Chinese).
6. Liu WX, Bu ZG. Prevention and control of brucellosis in China. Sci Sin Vitae 2023;53(12):1713 – 21. https://doi.org/10.1360/SSV-2023-0131.
7. Yu XL, Gao YX, Wang S, Fang M, Ding SJ, Kou ZQ. Epidemiological characteristics of brucellosis and its correlation with meteorological factors in Shandong Province from 2010 to 2021. Chin J Dis Control Prev 2025;29(5):580 – 7. https://doi.org/10.16462/j.cnki.zhjbkz.2025.05.013.
8. Professional Committee of Microbiology and Immunology, Xinjiang Medical Association, Professional Committee of Laboratory Medicine, Xinjiang Medical Association. Expert consensus on laboratory testing and clinical application of brucellosis. Lab Med Clin 2025;22(18):2449 – 57, 2463. https://doi.org/10.3969/j.issn.1672-9455.2025.18.001.
9. Zhang M. Study on the association between the prevalence of human brucellosis and socio-meteorological factors and meteorologically driven incidence prediction in China [dissertation]. Chongqing: Chongqing Medical University; 2024. http://dx.doi.org/10.27674/d.cnki.gcyku.2024.001436. (In Chinese).

SUPPLEMENTARY MATERIALS

SUPPLEMENTARY TABLE S1. Parameters and feature variables of SARIMA-XGBoost in the time-series analysis of brucellosis.

Variables	Details of parameters/features
SARIMA optimal params	p=0, d=1, q=1, P=0, D=1, Q=1, m=12
XGBoost input feature	Fitted values of SARIMA
XGBoost rolling window size search range (months)	K:[24,36,48,60,72]
XGBoost grid search range	max_depth:[1,2,3], learning_rate:[0.1,0.15,0.2], subsample:[0.6,0.7,0.8], nrounds<200, early_stopping_rounds=30
XGBoost optimal params	K=24, max_depth=1, learning_rate=0.2, subsample=0.6, nrounds=21

Abbreviation: SARIMA=seasonal autoregressive integrated moving average; XGBoost=extreme gradient boosting; RMSE=root mean square error; MAE=mean absolute error; MAPE=mean absolute percentage error.

SUPPLEMENTARY TABLE S2. Geodetector and collinearity tests for brucellosis-related influencing factors.

Factors	q	*P*	VIF
Sheep and goat inventory (10,000 head)	0.37	<0.01	2.54
Cattle and buffalo inventory (10,000 head)	0.12	<0.01	2.00
Average temperature (℃)	0.70	<0.01	2.44
Relative humidity (%)	0.39	<0.01	4.85
Average wind speed (m/s)	0.28	<0.01	3.78
Precipitation (100 mm)	0.18	<0.01	1.91
Number of medical technical personnels (10,000 person)	0.06	0.20	–
Number of rural doctors and health workers (10,000 person)	0.04	0.38	–

Note: Factor with q value>0.1, $P \leq 0.05$ and VIF≤5 are regarded as significant influencing factors, and are included in the following OLS and GTWR. "-" means indicates q value>0.1 and $P>0.05$, and these values are not displayed.
Abbreviation: VIF=variance inflation factor; OLS=ordinary least squares; GTWR=geographically and temporally weighted regression.

SUPPLEMENTARY TABLE S3. The model evaluation results of SARIMA and SARIMA-XGBoost in brucellosis related factor.

Model	Augmented Dickey-Fuller Test		Ljung-Box Test (lag=12)		RMSE	MAE	MAPE
	Dickey-Fuller	*P*	Ljung-Box Q				
SARIMA	-6.12	<0.01	8.43	0.75	0.09	0.08	31.86
SARIMA-XGBoost			13.17	0.36	0.08	0.07	26.74

Note: SARIMA parameters: (0,1,1)(0,1,1)12.
Abbreviation: RMSE=root mean squared error; MAE=mean absolute error; MAPE=mean absolute percentage error.

SUPPLEMENTARY TABLE S4. Model evaluation results of OLS and GTWR for brucellosis-related factors.

Model	R^2	Adjusted R^2	AICc	RSS
OLS	0.76	0.75	467.70	529.60
GTWR	0.82	0.78	466.77	395.95

Note: The optimal spatiotemporal bandwidth of GTWR is set to 21.
Abbreviation: R^2=coefficient of determination; AICc=corrected Akaike information criterion; RSS=residual sum of squares; OLS=ordinary least squares; GTWR=geographically and temporally weighted regression.

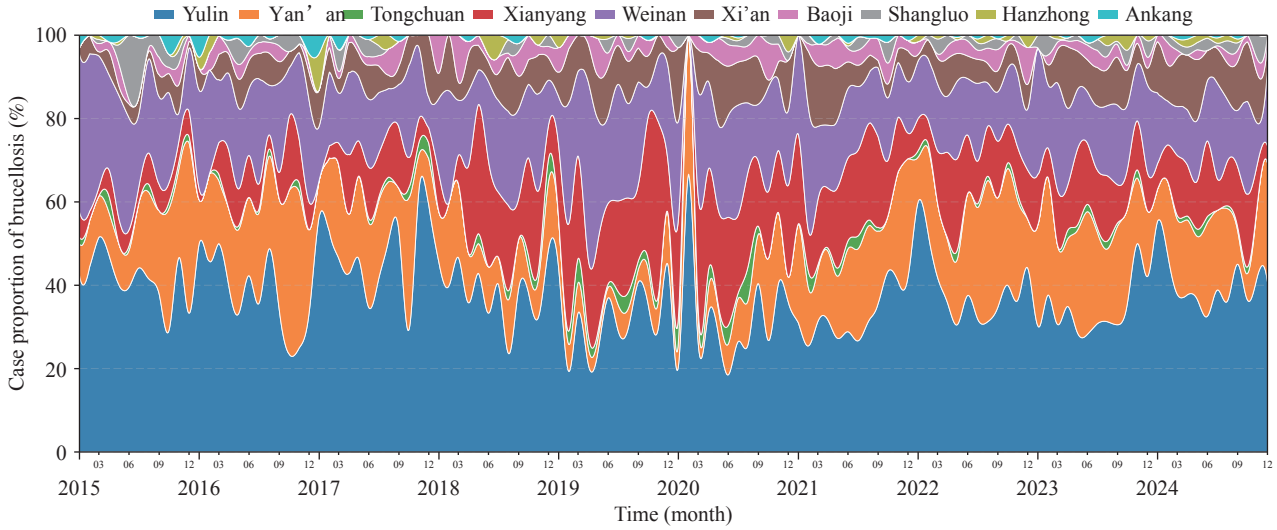

SUPPLEMENTARY FIGURE S1. Monthly distribution of brucellosis cases in prefectural cities across Shaanxi Province, 2015–2024.
Note: Municipalities directly under the province are not included in the statistics.

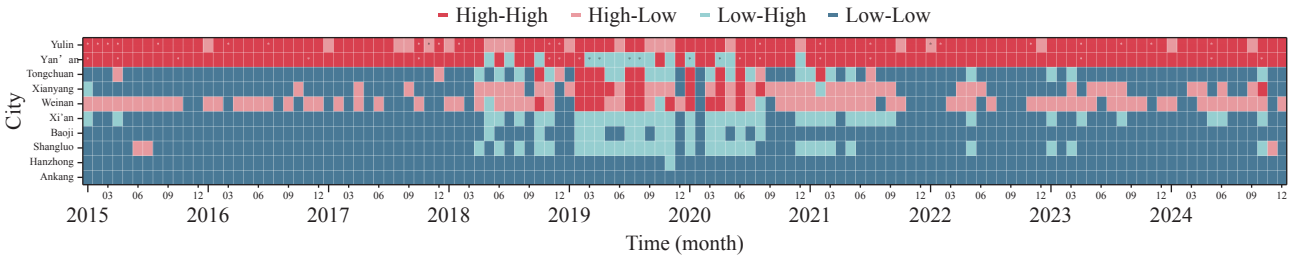

SUPPLEMENTARY FIGURE S2. Heat map of monthly local spatial clustering results for brucellosis in Shaanxi Province, 2015–2024.
Note: Municipalities directly under the province are not included in the statistics. * indicates statistical significance ($P \leq 0.05$).

Preplanned Studies

Financial Feasibility of BPaL(M) Under Pretomanid Price Scenarios — China, 2023–2024

Jingjuan Ren[1]; Ni Wang[1]; He Zhu[2]; Wenjuan Nie[3]; Feng Sun[4]; Yu Xiong[5]; Liang Fu[6]; Hui Luo[7]; Shiming Cheng[8]; Yanlin Zhao[1]; Fei Huang[1,#]

Summary

What is already known about this topic?

The BPaL(M) regimen is a World Health Organization (WHO)-endorsed, all-oral, shorter treatment for multidrug- or rifampicin-resistant tuberculosis (MDR/RR-TB) recently approved in China; however, its large-scale implementation depends on affordability and sustainability within the national health insurance system.

What is added by this report?

This study identifies 26,000 Chinese Yuan (CNY) per course as an approximate break-even pretomanid price for health insurance reimbursement in China. Lower prices can generate savings for both insurers and patients.

What are the implications for public health practice?

Pretomanid price negotiations should be combined with reimbursement and financial protection policies to support equitable scale-up of BPaL(M).

ABSTRACT

Introduction: The BPaL(M) regimen is a World Health Organization (WHO)-endorsed treatment for multidrug- or rifampicin-resistant tuberculosis (MDR/RR-TB). Its affordability and scale-up depend on pretomanid pricing. We assessed the economic impact of BPaL(M) under alternative pricing scenarios for both health insurance reimbursements and patients.

Methods: We conducted a cost survey among 50 patients with MDR/RR-TB in five TB-designated hospitals. We defined and collected direct medical, direct nonmedical, and indirect patient costs and used a budget impact tool to compare BPaL(M) regimens with current standard-of-care DR-TB regimens across four alternative pretomanid pricing scenarios.

Results: At 26,000 Chinese Yuan (CNY) per course, BPaL(M) saved 4,573 CNY per patient: 1 CNY for health insurance reimbursement (cost-neutral) and 4,572 CNY for patients. At 1,300 CNY per course, the total savings increased to 28,779 CNY per patient, with 14,524 CNY attributable to health insurance reimbursement and 14,255 CNY saved by patients. Over five years, 26,000 CNY per course yielded 265 million CNY total savings, with 80% accruing to patients.

Conclusion: 26,000 CNY per course is the break-even pretomanid price. Pricing aligned with global benchmarks generates savings. Pretomanid pricing at or below the break-even threshold is essential to support the sustainable scale-up of BPaL(M) and improve financial protection in China.

China has one of the largest global burdens of drug-resistant tuberculosis (TB). According to the Global Tuberculosis Report 2025, China was estimated to have approximately 28,000 cases of multidrug- or rifampicin-resistant TB (MDR/RR-TB, collectively referred to as DR-TB) in 2024, ranking second worldwide in absolute number of cases (*1*). Despite progress in TB control, DR-TB continues to pose substantial clinical, economic, and public health challenges. Treatment remains lengthy and burdensome; conventional MDR-TB regimens typically last 18–24 months and involve complex multidrug combinations, often including injectable agents. More recently, China has implemented a 9–12-month all-oral regimen incorporating bedaquiline, which represents an important therapeutic advancement. However, realizing population-level benefits critically depends on affordability and financial sustainability within the health insurance reimbursement system.

Therefore, drug pricing is a central concern, particularly given that DR-TB disproportionately affects lower-income and marginalized populations with a limited capacity to absorb high treatment costs.

Although public health insurance reimburses approximately 60%–80% of MDR-TB drug costs, the total drug price is approximately 56,400 Chinese Yuan (CNY), leaving patients responsible for co-payments of up to 22,500 CNY (*2*–*3*). This financial burden remains prohibitive for many patients and places considerable pressure on reimbursement budgets, thereby limiting access to newer regimens.

In 2022, the World Health Organization endorsed the 6-month BPaL(M) regimen (bedaquiline, pretomanid, and linezolid, with or without moxifloxacin) as the preferred treatment option owing to its higher efficacy and shorter duration. In December 2024, the National Medical Products Administration approved pretomanid (PA-824) for use in China, and the China CDC subsequently updated the treatment guidelines to include BPaL(M) for rifampicin-resistant TB (RR-TB), the main form of DR-TB. However, the clinical advantages of BPaL(M) may not translate into economic gains for the healthcare system or patients unless pretomanid is priced at a level that ensures reimbursement feasibility and affordability of patient-borne costs (PBC). High price risk limits scale-up, while increasing the pressure on health insurance expenditure.

Therefore, this study evaluates the economic impact of adopting BPaL(M) in China under multiple pretomanid price scenarios from both health insurance reimbursement and patient perspectives, with the aim of identifying a sustainable price threshold that supports broad access, reduces patient financial burden, and maintains the fiscal sustainability of pharmaceutical reimbursement.

A cross-sectional survey was conducted from 2023–2024 across five TB-designated hospitals in different regions of China (Beijing Chest Hospital, Huashan Hospital, Shandong Provincial Chest Hospital, Xi'an Chest Hospital, and Shenzhen Third People's Hospital). Hospitals were selected based on referral status, case volume, and geographic representation. At each hospital, ten patients with pulmonary DR-TB who had completed treatment within the past 12 months were randomly selected for physician-administered interviews. As DR-TB treatment in China follows strict national standardized clinical pathways, collecting cost data from a sample of 50 patients across five high-volume regional centers provides an initial real-world baseline for parameterizing the deterministic model. Because the BPaL(M) regimen has only recently been approved, large-scale real-world cost data are not yet available. Consequently, using conventional regimen costs as a baseline, adjusted by deterministic clinical pathway parameters (e.g., shorter duration and reduced monitoring based on national guidelines), serves as a reliable health-economic modeling approach before widespread programmatic scale-up. The collected data included demographic characteristics (e.g., age, sex, type of current address, monthly salary), direct medical costs (out-of-pocket co-payments for drugs, laboratory tests, and hospitalizations), direct non-medical costs (transportation, accommodation, and food), and indirect costs (income loss due to illness).

An economic evaluation was conducted using a costing tool developed by the Swiss Tropical and Public Health Institute (*4*). The model simulates patient treatment pathways across different regimen scenarios and their corresponding treatment costs. In this study, the tool was parameterized to reflect China's epidemiological and economic context. The analysis modeled four pricing scenarios for pretomanid: Scenario 1 (26,000 CNY per course): this price aligns with the current U.S. price of pretomanid and serves as an international reference; Scenario 2 (32,000 CNY per course): this scenario assumes a price 25% above the U.S. price, reflecting the potential higher pricing in China; Scenario 3 (1,300 CNY per course): this price reflects the Global Drug Facility (GDF) price available to over 150 low- and middle-income countries, serving as a global access benchmark; Scenario 4 (7,300 CNY per course): this price represents an approximately 70% markdown from the U.S. price, similar to the price reduction seen for bedaquiline at launch in China.

Although the price at which pretomanid will be launched in China is unknown, these scenarios were selected to capture both realistic and optimal price points. In each scenario, we assumed that China's public insurance would reimburse 60% of the pretomanid costs (similar to the initial reimbursement rate for bedaquiline). These scenarios were analyzed to evaluate their impact on the overall health system expenditures and PBC.

The model incorporated differences in treatment duration by calculating the total quantity of drug doses and the required frequency of laboratory monitoring and outpatient visits specific to the 6-month versus current regimens, which are in line with the latest national guidelines. The primary estimated indicators included: *Per-patient costs*, defined as the total financial expenditure incurred for a single completed treatment stratified by health insurance reimbursement and patient out-of-pocket expenditure; *Health insurance*

reimbursement, refers to costs covered by basic medical insurance; *PBC*, defined as the total direct and indirect financial burden placed on patients; and *Five-year budget impact*, defined as the aggregated net cost difference to the health system over five years based on China's CDC projections of BPaL(M) programmatic uptake.

At a pretomanid price of 26,000 CNY per course, BPaL(M) was cost neutral for health insurance reimbursement and cost savings for patients, with net savings of 4,573 CNY per patient. Increased medicine costs (3,931 CNY) were fully offset by reduced monitoring costs (3,932 CNY), resulting in a neutral budget impact for health insurance reimbursement, whereas patients benefited from reduced monitoring and hospitalization/travel costs, leading to a 4,572 CNY reduction in PBC. At 32,000 CNY per course, BPaL(M) generated additional costs for health insurance reimbursement (3,821 CNY per patient) despite modest patient savings (2,024 CNY per patient). If all eligible patients were treated with BPaL(M), this price point would result in an estimated 50.2 million CNY increase in the annual health insurance expenditure, limiting financial sustainability. At lower pretomanid prices, BPaL(M) was cost-effective. At 7,300 CNY per course, savings reached 10,921 CNY per patient for health insurance reimbursement and 11,852 CNY per patient for patients, corresponding to 143.5 million CNY in annual savings for the health insurance system. At a GDF price of 1,300 CNY per course, total savings increased to 28,779 CNY per patient, evenly shared between health insurance reimbursement (14,524 CNY) and patients (14,255 CNY), with potential annual health insurance savings of 191 million CNY (Table 1).

Break-even and budget impact analysis: Scenario analysis identified 26,000 CNY per course as the break-even threshold at which BPaL(M) neither increases nor decreases health insurance reimbursement expenditure, while substantially reducing the patient's financial burden. Prices above this level increase budgetary pressure, whereas prices below this level generate substantial system-wide savings. Over five years, the total savings were estimated at 265 million CNY at 26,000 CNY per course (approximately 80% accruing to patients), 923 million CNY at 7,300 CNY per course, and 1.14 billion CNY at 1,300 CNY per course, with lower prices creating significant fiscal space for reinvestment in DR-TB control programs (Figures 1–3).

DISCUSSION

The introduction of a short all-oral BPaL(M) regimen represents a major advance in the treatment of DR-TB. This study provides evidence of the financial feasibility of adopting BPaL(M) in China by examining multiple pretomanid price scenarios from both health insurance reimbursement and patient perspectives. Our findings demonstrate that the price of pretomanid is the primary determinant of the affordability and sustainability of the regimen. At the price of 32,000 CNY per course, the adoption of BPaL(M) would substantially increase health insurance reimbursement expenditures, limiting the feasibility of

TABLE 1. Main incremental per-patient cost components of BPaL(M) under different pretomanid price scenarios (CNY).

Pretomanid prices per course	Category	Cost type			Total incremental cost/saving
		Medicine costs	Laboratory/monitoring costs	Hospitalization/ travel-related costs	
26,000	Health insurance reimbursement	3,931	−3,932	−	−1
	PBC	1,321	−2,621	−3,272	−4,572
32,000	Health insurance reimbursement	7,753	−3,932	−	3,821
	PBC	3,869	−2,621	−3,272	−2,024
7,300	Health insurance reimbursement	−6,989	−3,932	−	−10,921
	PBC	−5,959	−2,621	−3,272	−11,852
1,300	Health insurance reimbursement	−10,593	−3,932	−	−14,524
	PBC	−8,361	−2,621	−3,272	−14,255

Note: A minus sign (−) indicates a reduction in costs (i.e., savings) compared to the standard of care; This table presents the main incremental cost components captured in the model. "Hospitalization/travel-related costs" refers to the aggregated change in patient costs related to hospitalization and treatment-related travel. Direct non-medical and indirect costs were collected in the survey and considered in the overall assessment of PBC, but are not separately itemized in this table.
Abbreviation: PBC=patient-borne costs; CNY=Chinese Yuan.

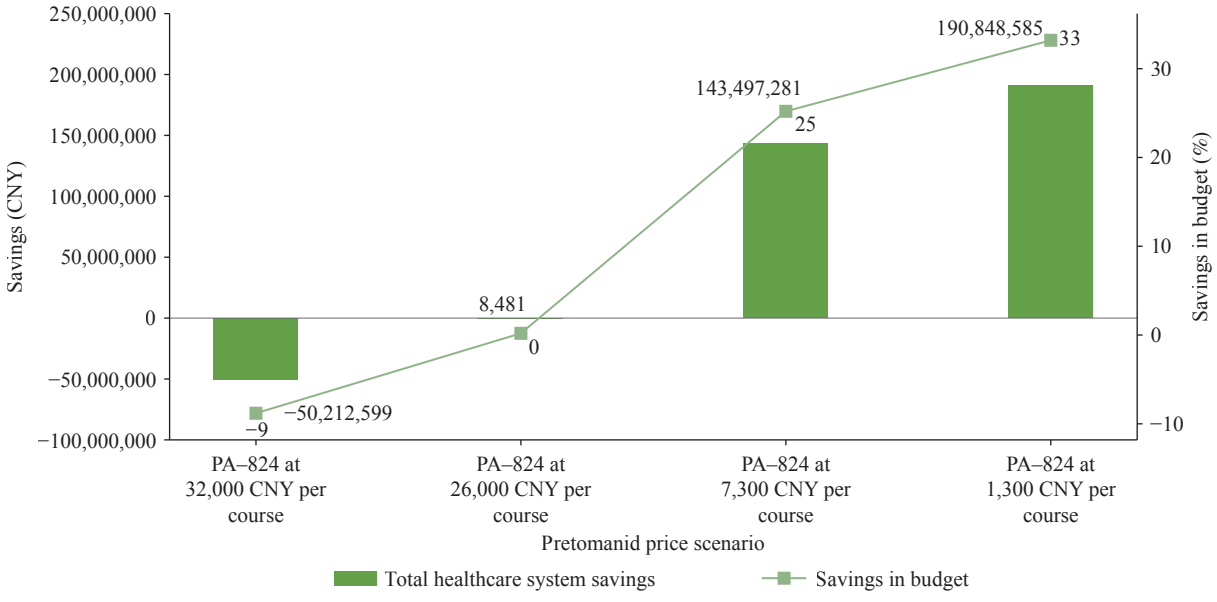

FIGURE 1. Annual healthcare budget impact of BPaL(M): savings, costs, and the break-even transition zone.
Abbreviation: CNY=Chinese Yuan.

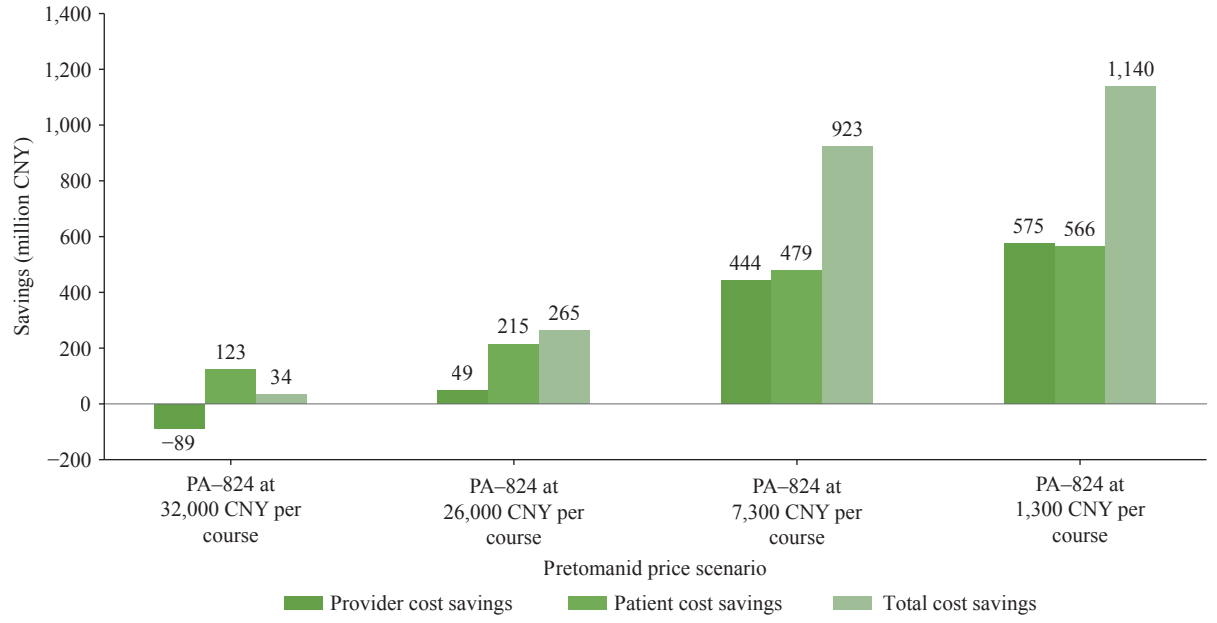

FIGURE 2. 5-year incremental savings (in million CNY) for BPaL(M).
Abbreviation: CNY=Chinese Yuan.

large-scale implementation. In contrast, a price of 26,000 CNY per course represents a critical break-even threshold at which BPaL(M) becomes budget-neutral for health insurance reimbursement, while substantially reducing PBC. Further price reductions generate increasingly large savings for both the health system and patients, supporting the economic rationale for scale-up.

These findings are consistent with international evidence showing that shorter and more effective DR-TB regimens can reduce the overall treatment costs by decreasing treatment duration, healthcare utilization, and indirect costs. Studies from South Africa, Georgia, and the Philippines have projected that BPaL(M) could be cost-effective for extensively drug-resistant TB treatment (*5*). Multi-country analyses have reported per-patient savings ranging from 112 US Dollars (USD) to 1,173 USD (*6*), while national-level

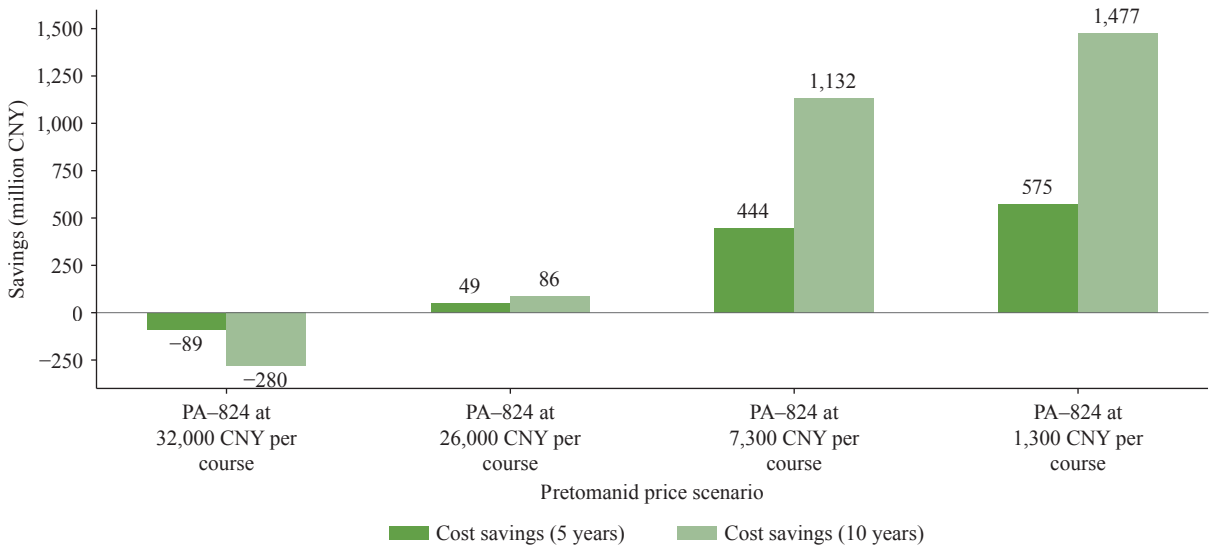

FIGURE 3. Health insurance reimbursement savings over time (million CNY) for BPaL(M).
Abbreviation: CNY=Chinese Yuan.

modeling in Moldova has estimated savings of 7.1 million USD over five years (*7*). Similar budgetary benefits have been reported in Indonesia, Kyrgyzstan, and Nigeria (*8*), as well as in a four-country analysis including Pakistan, the Philippines, South Africa, and Ukraine (*4*). Our results extend this evidence by demonstrating the interaction of pricing strategies with China's health insurance reimbursement system and patient cost-sharing mechanisms. While both our study and international models show that a shorter BPaL(M) duration significantly reduces non-medical and monitoring costs, their pricing environments differ critically. International studies assume heavily subsidized Global Drug Facility (GDF) prices that guarantee savings, whereas China's commercial pricing dynamics make net health system savings uncertain.

Importantly, our findings suggest that the break-even price of 26,000 CNY per course should be regarded as a negotiation ceiling rather than an optimal target. Although this price avoids an additional burden on the health insurance reimbursement system, it generates limited fiscal space for reinvestment. In contrast, lower pretomanid prices substantially expanded savings, creating opportunities to strengthen DR-TB programs through investments in diagnostics, adherence support, and service delivery. Given that pretomanids were developed by a nonprofit organization with a public health mandate, these findings support the alignment of pricing strategies with long-term affordability and access objectives.

Despite the substantial reductions in PBC observed under all pricing scenarios, financial hardships may persist, even at lower drug prices, if current reimbursement arrangements remain unchanged. Existing health insurance schemes in China provide incomplete protection for patients with DR-TB, particularly for outpatient services, and high copayments continue to contribute to catastrophic expenditures (*9*). Achieving universal access to BPaL(M) will therefore require complementary reforms in health financing policies alongside favorable drug pricing, including adjustments to reimbursement rates and benefit packages.

Beyond absolute cost reductions, the adoption of BPaL(M) has profound implications for achieving the WHO End TB Strategy goal for zero TB-affected households facing catastrophic costs. Our study shows that the BPaL(M) could be a catalyst for Universal Health Coverage (UHC) by shortening the "period of financial vulnerability" from 18–24 months to just 6 months. However, the risk of Catastrophic Health Expenditures (CHE) persists if outpatient reimbursement gaps are not addressed. Policymakers should consider a 'total-cost protection' model that goes beyond drug subsidies. This includes expanding the Special Disease outpatient benefit packages to cover 90% or more of DR-TB costs and integrating social protection mechanisms to offset non-medical expenses, such as nutritional support. Only by aligning drug pricing with comprehensive financing reforms can China translate the clinical efficacy of BPaL(M) into true financial protection for the most vulnerable population.

Finally, the standardized and short-duration nature

of the BPaL(M) regimen aligns well with the ongoing payment reforms in China, such as Diagnosis-Related Group-based payment systems. Evidence from Wuhan suggests that DRG implementation for DR-TB can reduce the total medical expenditure and length of hospital stay without shifting costs to patients (*10*). Integrating BPaL(M) into such payment models may further enhance efficiency and affordability.

This study had some limitations. Budget impact estimates are based on the projected five-year uptake of BPaL(M) and may differ from real-world implementations. Patient cost data were derived from a small multisite sample, limiting generalizability and introducing potential recall bias. Although the key model assumptions were informed by available clinical practice, hospital data, published evidence, and expert consultation, some parameters, including monitoring frequency and service utilization, may vary across regions and institutions. In addition, the analysis did not capture broader societal benefits, such as reduced transmission or quality-of-life gains, which may have led to the underestimation of long-term economic benefits.

In conclusion, the financial feasibility of the BPaL(M) regimen in China depends primarily on the price of pretomanid. The price of 26,000 CNY per course represents a cost-neutral threshold for the health insurance reimbursement system and supports near-term adoption. However, lower prices aligned with global access benchmarks are needed to maximize reductions in patients' financial burden and support sustained progress toward national and global DR-TB control goals. Therefore, securing an affordable pretomanid price is essential to enable broad access to BPaL(M) and translate clinical advances into durable public health and economic benefits in China.

Conflicts of interest: No conflicts of interest.

Ethical statement: Approved by the ethics committees of the participating hospitals and written informed consent was obtained from all participants.

doi: 10.46234/ccdcw2026.106

[#] Corresponding author: Fei Huang, huangfei@chinacdc.cn.

[1] National Key Laboratory of Intelligent Tracking and Forecasting for Infectious Diseases, National Center for Tuberculosis Control and Prevention, Chinese Center for Disease Control and Prevention & Chinese Academy of Preventive Medicine, Beijing, China; [2] School of Public Health, Peking University, Beijing, China; [3] Department of Tuberculosis, Beijing Chest Hospital, Capital Medical University, Beijing, China; [4] National Medical Center for Infectious Diseases, Huashan Hospital, Fudan University, Shanghai, China; [5] Department of Tuberculosis, Public Health Clinical Center Affiliated to Shandong University, Jinan City, Shandong Province, China; [6] Division Two of Pulmonary Diseases Department, Shenzhen Third People's Hospital, Shenzhen Clinical Research Center for Tuberculosis, National Clinical Research Center for Infectious Disease (Shenzhen), Southern University of Science and Technology, Shenzhen City, Guangdong Province, China; [7] Department of Drug-Resistance Tuberculosis, Xi'an Chest Hospital, Xi'an City, Shaanxi Province, China; [8] Chinese Antituberculosis Association, Beijing, China.

Submitted: February 10, 2026
Accepted: May 11, 2026
Issued: May 22, 2026

REFERENCES

1. World Health Organization. Global tuberculosis report 2025. Geneva: World Health Organization; 2025. https://www.who.int/teams/global-programme-on-tuberculosis-and-lung-health/tb-reports/global-tuberculosis-report-2025. [2026-02-8].
2. TB Alliance. Price of key DR-TB medicine drops 25% as TB Alliance's multi-manufacturer strategy expands access. https://www.tballiance.org/price-of-key-dr-tb-medicine-drops-25-as-tb-alliances-multi-manufacturer-strategy-expands-access/. [2026-02-8].
3. Conradie F, Diacon AH, Ngubane N, Howell P, Everitt D, Crook AM, et al. Treatment of highly drug-resistant pulmonary tuberculosis. N Engl J Med 2020;382(10):893 – 902. https://doi.org/10.1056/NEJMoa1901814.
4. Auer C, Gupta A, Malbacius C, Ghafoor A, Kock Y, Medvedieva O, et al. Savings from the introduction of BPaL and BPaLM regimens at the country level. IJTLD Open 2024;1(7):314 – 9. https://doi.org/10.5588/ijtldopen.24.0213.
5. Gomez GB, Siapka M, Conradie F, Ndjeka N, Garfin AMC, Lomtadze N, et al. Cost-effectiveness of bedaquiline, pretomanid and linezolid for treatment of extensively drug-resistant tuberculosis in South Africa, Georgia and the Philippines. BMJ Open 2021;11(12):e051521. https://doi.org/10.1136/bmjopen-2021-051521.
6. Sweeney S, Berry C, Kazounis E, Motta I, Vassall A, Dodd M, et al. Cost-effectiveness of short, oral treatment regimens for rifampicin resistant tuberculosis. PLoS Glob Public Health 2022;2(12):e0001337. https://doi.org/10.1371/journal.pgph.0001337.
7. James LP, Klaassen F, Sweeney S, Furin J, Franke MF, Yaesoubi R, et al. Impact and cost-effectiveness of the 6-month BPaLM regimen for rifampicin-resistant tuberculosis in Moldova: a mathematical modeling analysis. PLoS Med 2024;21(5):e1004401. https://doi.org/10.1371/journal.pmed.1004401.
8. Mulder C, Rupert S, Setiawan E, Mambetova E, Edo P, Sugiharto J, et al. Budgetary impact of using BPaL for treating extensively drug-resistant tuberculosis. BMJ Glob Health 2022;7(1):e007182. https://doi.org/10.1136/bmjgh-2021-007182.
9. Tang SL, Wang LX, Wang H, Chin DP. Access to and affordability of healthcare for TB patients in China: issues and challenges. Infect Dis Poverty 2016;5:10. https://doi.org/10.1186/s40249-016-0096-y.
10. Xiong YB, Yao YF, Li YH, Chen SQ, Li YF, Lin KH, et al. Impact of diagnosis-related group payment on medical expenditure and treatment efficiency on people with drug-resistant tuberculosis: a quasi-experimental study design. Int J Equity Health 2025;24(1):1. https://doi.org/10.1186/s12939-024-02368-0.

Preplanned Studies

Rotavirus Vaccine Coverage in a Birth Cohort — China, 2019–2023

Yingxia Li[1,2,3]; Yifan Song[2,3]; Zhaonan Zhang[2,3]; Li Li[2,3]; Likun Shi[4]; Jiayu He[5]; Lei Cao[2,3]; Wenzhou Yu[2,3]; Zundong Yin[2,3]; Jiakai Ye[2,3,#]

Summary

What is already known about this topic?

Rotavirus causes severe acute gastroenteritis and diarrhea-related mortality in children aged <5 years. Vaccination is an effective preventive strategy; however, no nationwide data on rotavirus vaccine coverage are available.

What is added by this report?

Based on data from the National Immunization Program Information System, despite the upward trend, rotavirus vaccine coverage among children born between 2019 and 2023 in China remained low, with suboptimal series completion. Disparities by socioeconomic region and clinic density were observed for non-National Immunization Program (non-program) childhood vaccines.

What are the implications for public health practice?

Improving follow-up for children with missed rotavirus vaccine doses, optimizing the distribution and accessibility of vaccination clinics, and exploring non-program-funded financing mechanisms for vaccination may improve rotavirus vaccine uptake.

ABSTRACT

Introduction: Rotavirus is the leading cause of severe acute gastroenteritis and diarrhea-related mortality in children aged <5 years. This study estimated rotavirus vaccination coverage in the 2019–2023 birth cohorts in China and provided a reference for improving coverage.

Methods: Individual-level data were obtained from the National Immunization Program Information System on the number of children born between 2019 and 2023, the number of rotavirus vaccine doses administered, and the number of vaccination clinics providing non-National Immunization Program (non-program) childhood vaccines. A descriptive analysis of coverage by birth cohort, regional per capita disposable income, and density of clinics providing non-program childhood vaccines was performed.

Results: From 2019 to 2023, the overall coverage of the first, second, and third doses of the rotavirus vaccine was 37.8%, 26.4%, and 19.4%, respectively, demonstrating an increasing trend across birth cohorts. Regions with the highest per-capita income had the highest coverage (44.4%, 33.1%, and 25.3%, respectively). Coverage was higher in areas with higher densities of clinics providing non-program childhood vaccines (40.5%, 29.6%, and 22.7%, respectively).

Conclusion: Rotavirus vaccine coverage in China was suboptimal. Improving follow-up for children with missed doses, optimizing the distribution of vaccination clinics, and exploring non-program-funded financing mechanisms for vaccination may improve rotavirus vaccine uptake.

Rotaviruses are a leading cause of severe diarrhea and mortality in infants and young children (*1*). China has the largest number of childhood deaths and economic burden of rotavirus diarrhea among Asian countries (*2*). No rotavirus-specific medications exist, and vaccination is the most effective method for preventing rotavirus gastroenteritis (*2*). Three vaccines are used in China: the Lanzhou lamb rotavirus vaccine (LLR), pentavalent human-bovine reassortant rotavirus vaccine (RV5), and trivalent oral human-lamb reassortant rotavirus vaccine (LLR3). The LLR, RV5, and LLR3 are not included in the National Immunization Program (non-program vaccines) and are paid for voluntarily by families. This study analyzed the vaccine coverage among children born between 2019 and 2023 in China to inform efforts to improve their uptake.

Data on the annual number of births, rotavirus vaccine doses administered, and the number of vaccination clinics providing non-program childhood vaccines were obtained from the National Immunization Program Information System (NIPIS) on October 30, 2025. Data on per-capita disposable

income were obtained from the China Statistical Yearbook (2023 Edition), and on provincial land area from official provincial government websites for 2023.

The vaccines used in this study were LLR and RV5. LLR was approved in China in 2000 (*3*) and is indicated for infants aged 2–3 years. It is administered orally once a year, in up to 3 doses. RV5 was approved in China in 2018 (*3*) and is indicated for infants aged 6–32 weeks in a 3-dose oral series. The first dose is administered between 6 and 12 weeks of age, with a 4–10-week interval between doses, and the third dose is administered no later than 32 weeks of age.

Coverage indicators were calculated as follows: 1) overall coverage for a specific dose of rotavirus vaccine in a given birth cohort (%) = (number of children in a given birth cohort who received that dose of LLR or RV5) / (total number of children in that birth cohort) × 100%; 2) coverage for a specific dose of LLR or RV5 in a given birth cohort (%) = (number of children in that birth cohort who received a dose of LLR or RV5) / (total number of children in that birth cohort) × 100%; and 3) density of clinics providing non-program childhood vaccines in a given region (clinics per 10,000 km^2) = (number of clinics providing non-program vaccines for children in that region) / (land area of that region).

Microsoft Office Excel (version 2010, Microsoft Corporation, Redmond, WA, USA) and SPSS (version 25.0, IBM Corp, Armonk, NY, USA) were used to analyze rotavirus vaccination status. Per capita disposable income was used to reflect economic level, with provinces categorized into low [<30,000 Chinese Yuan/year (CNY/year)], middle (30,000–39,999 CNY/year), and high (≥40,000 CNY/year) income groups. The density of clinics providing non-program childhood vaccines was used to reflect service accessibility, with provinces categorized into low (<70 clinics/10,000 km^2), middle (70–119 clinics/10,000 km^2), and high (≥120 clinics/10,000 km^2) density groups. The chi-square test was used to assess trends across birth cohorts, per capita disposable income levels, and regions with varying clinic densities. Spearman's correlation analysis was conducted to assess the correlation between rotavirus vaccination coverage, per capita disposable income, and the density of clinics offering non-program childhood vaccines. Statistical significance was set at $P<0.05$.

A total of 56.0721 million children born between 2019 and 2023 in NIPIS were enrolled in this study. From 2019 to 2023, the overall coverage of the first, second, and third doses of the rotavirus vaccine was 37.8%, 26.4%, and 19.4%, respectively. This indicates an upward trend across birth cohorts (all *P* for the trend across the three doses were < 0.001). Coverage for the first and second doses of LLR decreased from 24.4% and 10.7% in the 2019 birth cohort to 7.2% and 1.2% in the 2023 birth cohort, third-dose coverage decreased from 3.0% in the 2019 birth cohort to 0.7% in the 2022 birth cohort (all *P* for trend of the three doses were <0.001). RV5 coverage increased from 7.9%, 6.8%, and 6.0% in the 2019 birth cohort to 29.6%, 28.1%, and 26.4% in the 2023 birth cohort, respectively (all *P* for the trend of the three doses were <0.001) (Table 1 and Figure 1).

LLR and RV5 coverage were positively associated with higher regional per-capita disposable income (all *P* for the trends of the three doses were <0.001, with r_s ranging from 0.436 to 0.715). In high-income areas, the overall coverage was 44.4%, 33.1%, and 25.3% by dose; LLR coverage was 19.1%, 9.1%, and 3.3% for the three doses; and RV5 coverage was 25.3%, 24.0%, and 22.5%, respectively (Table 2).

LLR and RV5 coverage were positively associated with greater density of vaccination clinics providing non-program childhood vaccines (all *P* for the trend across the three doses were <0.05, with r_s ranging from 0.434 to 0.727). In high-density areas, the overall coverage was 40.5%, 29.6%, and 22.7% by dose. LLR coverage was the highest in middle-density areas at 22.0%, 9.8%, and 3.1% by dose, whereas RV5 coverage reached 23.7%, 22.0%, and 20.5% by dose in high-density areas, respectively (Tables 3 and 4).

DISCUSSION

Nationwide coverage for all three doses of the rotavirus vaccine increased annually among the 2019–2023 birth cohorts; LLR coverage declined with the introduction of RV5, possibly attributable to the earlier initial dose and shorter RV5 course. The complete LLR schedule extends to the age of 3 years; rotavirus primarily affects younger children, and the World Health Organization does not recommend vaccination for children over 24 months (*2*). By contrast, the newly introduced LLR3 vaccine, approved in 2023, offers an improved schedule.

Despite this increasing trend, first-dose coverage was below the global average, indicating a low rotavirus vaccine initiation rate in China (*4*). The series completion rates were suboptimal for both LLR and RV5, with LLR rates lower than those for RV5, possibly due to factors such as economic level, service

TABLE 1. Rotavirus vaccination coverage among children in birth cohorts from 2019 to 2023.

Birth year	No. of children (×10^4)	Overall						LLR						RV5					
		Dose 1		Dose 2		Dose 3		Dose 1		Dose 2		Dose 3		Dose 1		Dose 2		Dose 3	
		No. vaccinated (×10^4)	Coverage (%)	No. vaccinated (×10^4)	Coverage (%)	No. vaccinated (×10^4)	Coverage (%)	No. vaccinated (×10^4)	Coverage (%)	No. vaccinated (×10^4)	Coverage (%)	No. vaccinated (×10^4)	Coverage (%)	No. vaccinated (×10^4)	Coverage (%)	No. vaccinated (×10^4)	Coverage (%)	No. vaccinated (×10^4)	Coverage (%)
Total	5,607.21	2,119.70	37.8	1,481.10	26.4	1,088.42	19.4	1,002.92	17.9	441.64	7.9	122.91	2.6	1,116.79	19.9	1,039.46	18.5	965.51	17.2
2019	1,479.40	477.62	32.3	258.53	17.5	132.97	9.0	361.37	24.4	157.62	10.7	44.62	3.0	116.25	7.9	100.91	6.8	88.36	6.0
2020	1,219.87	465.37	38.1	311.64	25.5	212.50	17.4	261.97	21.5	126.40	10.4	41.94	3.4	203.40	16.7	185.25	15.2	170.56	14.0
2021	1,064.07	450.09	42.3	337.68	31.7	256.46	24.1	191.74	18.0	95.20	8.9	29.40	2.8	258.35	24.3	242.48	22.8	227.06	21.3
2022	963.60	403.52	41.9	315.68	32.8	254.12	26.4	124.87	13.0	51.79	5.4	6.96	0.7	278.65	28.9	263.88	27.4	247.16	25.7
2023	880.27	323.10	36.7	257.58	29.3	232.37	26.4	62.96	7.2	10.63	1.2	–*	–*	260.14	29.6	246.94	28.1	232.37	26.4
χ^2		121,164.75		682,870.34		1,553,470.06		1,358,945.53		790,777.07		110,146.62		2,375,460.68		2,414,649.39		2,360,279.07	
P for trend		<0.001		<0.001		<0.001		<0.001		<0.001		<0.001		<0.001		<0.001		<0.001	

Abbreviation: LLR=Lanzhou lamb rotavirus vaccine; RV5=pentavalent human-bovine reassortant rotavirus vaccine.

* The vaccination rate for the third dose of LLR in the 2023 birth cohort could not be calculated because the scheduled administration date fell after December 31, 2024 (data cutoff date).

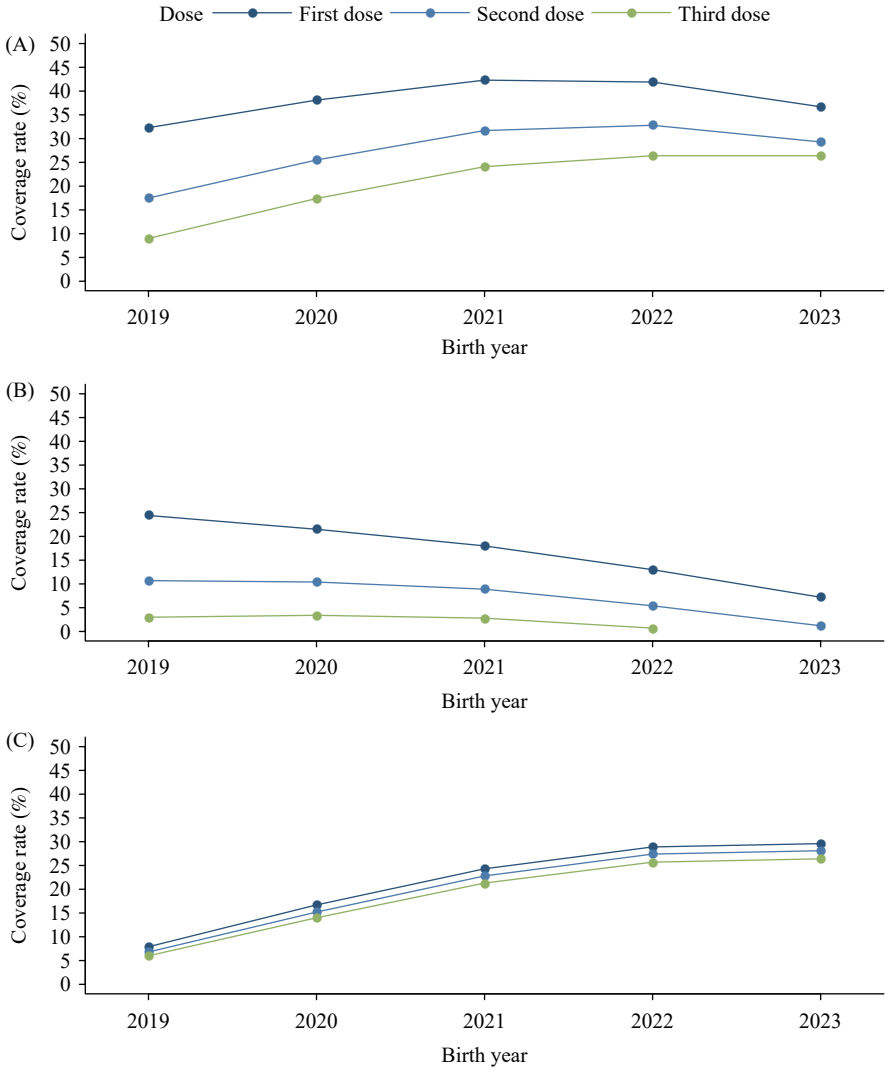

FIGURE 1. Rotavirus vaccine coverage by birth cohort, 2019–2023. (A) Overall Rotavirus vaccines; (B) LLR; (C) RV5. Abbreviation: LLR=Lanzhou lamb rotavirus vaccine; RV5=pentavalent human-bovine reassortant rotavirus vaccine.

accessibility, and maternal education (*5*). The lower LLR completion rate may be due to the longer interval between doses, which guardians may easily overlook (*6*).

Coverage was positively associated with higher regional per capita disposable income, consistent with previous findings (*7*). A study in Japan showed that lower household income and relative poverty were associated with reduced rotavirus vaccine coverage prior to free vaccination (*8*). Similarly, a randomized controlled trial in Hong Kong, China, showed that rotavirus vaccine coverage increased when vaccination was free (*9*). Previous studies (*7*–*9*) highlight the role of economic factors in improving rotavirus vaccine coverage.

The density of vaccination clinics providing non-program childhood vaccines was associated with higher coverage, highlighting the importance of vaccine accessibility. Currently, 13.4% of routine childhood vaccination clinics nationwide do not provide non-program childhood vaccines (*10*).

Clinics providing non-program childhood vaccines are concentrated in central urban areas; remote regions have relatively fewer such clinics (*11*). While increasing rotavirus vaccination services, the spatial balance of service distribution should be considered to improve the accessibility of non-program vaccines.

This study has some limitations. Data were from NIPIS. Owing to underreporting or delayed uploads, some cases might not have been included. In evaluating service accessibility, the density of clinics providing non-program childhood vaccines was calculated using the clinic-to-land area ratio, without accounting for transportation or travel modes.

TABLE 2. Rotavirus vaccination coverage in birth cohorts (2019–2023) by regional per capita disposable income.

Per capita disposable income	No. of children (×10^4)	Overall						LLR						RV5					
		Dose 1		Dose 2		Dose 3		Dose 1		Dose 2		Dose 3		Dose 1		Dose 2		Dose 3	
		No. vaccinated (×10^4)	Coverage (%)	No. vaccinated (×10^4)	Coverage (%)	No. vaccinated (×10^4)	Coverage (%)	No. vaccinated (×10^4)	Coverage (%)	No. vaccinated (×10^4)	Coverage (%)	No. vaccinated (×10^4)	Coverage (%)	No. vaccinated (×10^4)	Coverage (%)	No. vaccinated (×10^4)	Coverage (%)	No. vaccinated (×10^4)	Coverage (%)
Total	5,607.21	2,119.70	37.8	1,481.10	26.4	1,088.42	19.4	1,002.92	17.9	441.64	7.9	122.91	2.6	1,116.79	19.9	1,039.46	18.5	965.51	17.2
Low	1,545.95	456.98	29.6	289.23	18.7	207.64	13.4	234.32	15.2	86.62	5.6	21.82	1.7	222.66	14.4	202.60	13.1	185.82	12.0
Middle	2,495.26	967.22	38.8	673.34	27.0	484.99	19.4	468.95	18.8	211.84	8.5	57.92	2.7	498.27	20.0	461.51	18.5	427.07	17.1
High	1,565.99	695.50	44.4	518.53	33.1	395.79	25.3	299.65	19.1	143.18	9.1	43.17	3.3	395.85	25.3	375.35	24.0	352.62	22.5
χ^2		728,986.80		829,636.20		697,466.52		83,441.46		133,867.14		79,915.19		576,758.77		608,000.78		601,532.75	
P for trend		<0.001		<0.001		<0.001		<0.001		<0.001		<0.001		<0.001		<0.001		<0.001	

Abbreviation: LLR=Lanzhou lamb rotavirus vaccine; RV5=pentavalent human-bovine reassortant rotavirus vaccine.

TABLE 3. Rotavirus vaccination coverage in birth cohorts by density of vaccination clinics providing non-program childhood vaccines, 2019–2023.

Density of vaccination clinics providing non-program childhood vaccines	No. of children (×10^4)	Overall						LLR						RV5					
		Dose 1		Dose 2		Dose 3		Dose 1		Dose 2		Dose 3		Dose 1		Dose 2		Dose 3	
		No. vaccinated (×10^4)	Coverage (%)	No. vaccinated (×10^4)	Coverage (%)	No. vaccinated (×10^4)	Coverage (%)	No. vaccinated (×10^4)	Coverage (%)	No. vaccinated (×10^4)	Coverage (%)	No. vaccinated (×10^4)	Coverage (%)	No. vaccinated (×10^4)	Coverage (%)	No. vaccinated (×10^4)	Coverage (%)	No. vaccinated (×10^4)	Coverage (%)
Total	5,607.21	2,119.70	37.8	1,481.10	26.4	1,088.42	19.4	1,002.92	17.9	441.64	7.9	122.91	2.6	1,116.79	19.9	1,039.46	18.5	965.51	17.2
Low	1,293.23	383.84	29.7	251.93	19.5	177.21	13.7	201.34	15.6	82.99	6.4	22.11	2.0	182.51	14.1	168.94	13.1	155.10	12.0
Middle	1,447.80	574.41	39.7	380.11	26.3	261.10	18.0	318.22	22.0	141.49	9.8	38.39	3.1	256.19	17.7	238.61	16.5	222.70	15.4
High	2,866.18	1,161.46	40.5	849.06	29.6	650.11	22.7	483.36	16.9	217.15	7.6	62.40	2.6	678.10	23.7	631.91	22.0	587.71	20.5
χ^2		383,038.60		456,591.00		482,768.85		8.59		3,913.24		4,799.58		560,425.57		523,079.32		493,721.39	
P for trend		<0.001		<0.001		<0.001		0.003		<0.001		<0.001		<0.001		<0.001		<0.001	

Abbreviation: LLR=Lanzhou lamb rotavirus vaccine; RV5=pentavalent human-bovine reassortant rotavirus vaccine.

TABLE 4. Spearman's correlation coefficients between Rotavirus vaccination coverage and the corresponding variables.

Rotavirus vaccination coverage	Per capita disposable income		Density of vaccination clinics providing non-program childhood vaccines	
	r_s	*P*	r_s	*P*
Overall				
Dose 1	0.629	<0.001	0.646	<0.001
Dose 2	0.714	<0.001	0.702	<0.001
Dose 3	0.742	<0.001	0.736	<0.001
LLR				
Dose 1	0.436	0.014	0.434	0.015
Dose 2	0.529	0.002	0.520	0.003
Dose 3	0.518	0.003	0.513	0.003
RV5				
Dose 1	0.700	<0.001	0.727	<0.001
Dose 2	0.713	<0.001	0.717	<0.001
Dose 3	0.715	<0.001	0.714	<0.001

Abbreviation: LLR=Lanzhou lamb rotavirus vaccine; RV5=pentavalent human-bovine reassortant rotavirus vaccine; r_s=Spearman's rank correlation coefficient.

Accessibility may be overestimated in regions with complex terrain and poor transportation infrastructure.

In conclusion, the rotavirus vaccine coverage among children in China is low, with suboptimal series completion rates. Regional economic level and density of non-program childhood vaccination services were positively associated with coverage. To increase coverage, nudge-based strategies, such as intelligent voice calls and text messages, can improve the delivery of reminders and follow-ups for missed doses. Multichannel financing strategies, including government subsidies, free vaccination programs, and personal medical insurance accounts, should be explored to reduce costs and minimize the family's economic impact. Areas with low clinic densities should encourage routine vaccination clinics to offer non-program childhood vaccines, establish clinics in secondary and higher-level institutions, and use mobile units to reach remote areas. The distribution of clinics should be planned according to population density and service radius to enhance access.

Conflicts of interest: No conflicts of interest.

doi: 10.46234/ccdcw2026.107

[#] Corresponding author: Jiakai Ye, yejk@chinacdc.cn.

[1] Changsha Center for Disease Control and Prevention (Changsha Health Inspection Institute), Changsha City, Hunan Province, China; [2] National Key Laboratory of Intelligent Tracking and Forecasting for Infectious Diseases, Chinese Center for Disease Control and Prevention & Chinese Academy of Preventive Medicine, Beijing, China; [3] National Immunization Program, Chinese Center for Disease Control and Prevention & Chinese Academy of Preventive Medicine, Beijing, China; [4] Quanzhou Center for Disease Control and Prevention (Quanzhou Health Inspection Institute), Quanzhou City , Fujian Province, China; [5] Xinzhou Center for Disease Control and Prevention (Xinzhou Health Inspection Institute), Xinzhou City, Shanxi Province, China.

Submitted: March 26, 2026
Accepted: May 13, 2026
Issued: May 22, 2026

REFERENCES

1. GBD Diarrhoeal Diseases Collaborators. Estimates of global, regional, and national morbidity, mortality, and aetiologies of diarrhoeal diseases: a systematic analysis for the Global Burden of Disease Study 2015. Lancet Infect Dis 2017;17(9):909 – 48. https://doi.org/10.1016/S1473-3099(17)30276-1.
2. World Health Organization. Rotavirus vaccines: WHO position paper – July 2021. Wkly Epidemiol Rec 2021;96(28):301-19. https://www.who.int/publications/i/item/WHO-WER9628.
3. Writing Group for Expert Consensus on Rotavirus Gastroenteritis. Expert consensus on immunoprophylaxis of childhood rotavirus gastroenteritis (2024 version). Chin J Vaccines Immun 2024;30(1):95 – 126. https://doi.org/10.19914/j.CJVI.2024018.
4. World Health Organization. WHO immunization data portal – detail page. https://immunizationdata.who.int/global/wiise-detail-page. [2025-12-19].
5. Tahrat H, Munir A, Marchetti F. Rotavirus vaccine coverage, completion, and compliance: a systematic literature review. Hum Vaccin Immunother 2025;21(1):2442780. https://doi.org/10.1080/21645515.2024.2442780.
6. Li L, Liu N, Huang RN, Zhang LZ. Vaccination status of domestic rotavirus vaccine in Chengdu city. Int J Virol 2020;27(4):313 – 6. https://doi.org/10.3760/cma.j.issn.1673-4092.2020.04.012.
7. Liu Y, Yue CY, Li Y, Wang YM, Gao SR, Wang ZG, et al. Analysis of vaccination situation of orial live attenuated rotavirus vaccine (LLR strain) among children in 6 provinces of China. Chin J Prev Med

2018;52(3):282 – 6. https://doi.org/10.3760/cma.j.issn.0253-9624.2018.03.012.
8. Hara M, Koshida R, Araki K, Kondo M, Hirota Y. Determinants of self-paid rotavirus vaccination status in Kanazawa, Japan, including socioeconomic factors, parents' perception, and children's characteristics. BMC Infect Dis 2020;20(1):712. https://doi.org/10.1186/s12879-020-05424-6.
9. Yeung KHT, Yeung CCW, Tam WH, Liu KS, Fung GPG, Nelson EAS. Multiple-component interventions to increase rotavirus vaccine uptake in children: a randomised controlled trial. Lancet Reg Health West Pac 2024;50:101153. https://doi.org/10.1016/j.lanwpc.2024.101153.
10. Ye JK, Cao L, Yu WZ, Yin ZD. Current situation and resource allocation of routine vaccination units in China, 2021. Pract Prev Med 2023;30(7):789 – 94. https://doi.org/10.3969/j.issn.1006-3110.2023.07.005.
11. Ye LX, Fang T, Ma R, Dong HJ, Xu GZ. Spatial clustering of services of adult vaccination clinics in Ningbo city of Zhejiang province. Chin J Vaccines Immun 2018;24(1):89 – 94,111. https://doi.org/10.19914/j.cjvi.2018.01.021.

Perspectives

Between Achievement and Challenge: Examining China's Tuberculosis Control Pathway and Future Directions from a Global Perspective

Yanqiu Zhang[1]; Dingyong Sun[1]; Linqi Diao[1,#]

ABSTRACT

The *World Health Organization (WHO) Global Tuberculosis Report 2025* (*the Report*) was released on November 12, 2025, covering disease burden, diagnosis and treatment, prevention and screening, financing, universal health coverage (UHC), multisectoral accountability, research and innovation, and provides the latest benchmark for global tuberculosis (TB) prevention and control. *The Report* indicates that China's incidence rate has, for the first time, entered the category of lower moderate-burden countries. China has made significant progress in expanding coverage of rapid diagnostic technologies and increasing domestic financing. Its strategy and implementation model for scaling up TB preventive treatment (TPT) have been recognized as an international best practice, although current coverage among household contacts remains below the global average. However, global comparisons also reveal that China continues to face challenges in narrowing the case detection gap, improving the bacteriological positivity rate, addressing the high burden of drug-resistant (DR) TB, and mitigating the economic risks for affected households. These challenges are similar to those in high-burden countries. This perspective uses *the Report*'s structured framework to conduct a systematic comparative analysis of global trends and China's TB control landscape. It aims to review China's achievements and challenges and, drawing on global consensus and local practices, propose strategic priority actions necessary for China to advance toward the goal of ending the TB epidemic.

THE GLOBAL TB EPIDEMIC AND CHINA'S POSITION

The *Global Tuberculosis Report 2025* (*the Report*) (*1*) indicates that global tuberculosis (TB) control is at a critical turning point. Following the impact of the COVID-19 pandemic, the estimated global TB incidence rate stood at 131 cases per 100,000 population in 2024, marking a marginal decrease of approximately 2% for the first time, with an estimated 10.7 million new cases. However, this progress remains fragile and uneven, and a significant gap remains in achieving the ambitious goal of ending the TB epidemic.

The estimated TB incidence rate in China was 49 per 100,000 population in 2024 (approximately 696,000 cases). China has dropped from third to fourth place among the 30 high TB burden countries, and its incidence rate has entered the lower moderate-burden category for the first time, demonstrating China's contribution to global TB control and prevention. Within the global context, China's position remains pivotal. TB cases in China account for approximately 6.5% of cases globally. However, in the more severe domain of multidrug-resistant or rifampicin-resistant TB (MDR/RR-TB), China ranks second-highest globally, contributing 7.1% of MDR/RR-TB cases. China faces the complex task of ensuring rapid diagnosis and effective, affordable treatment for drug-resistant cases. The effectiveness of its control efforts will directly influence global MDR/RR-TB trends, underscoring both its responsibility and challenges.

The Report categorizes global response actions into six core components. Table 1 presents key indicators for both global and Chinese contexts.

CHINA'S SUCCESSFUL EXPERIENCE AND THE CHALLENGES IT FACES

China's Contributions and Challenges in Diagnostic Capacity and Drug-resistant TB Treatment

Microbiological detection of TB enables accurate

TABLE 1. Comparative analysis of global TB indicators and China's status (2024).

WHO report domain	Global indicators/context	China's corresponding status/position
Disease Burden	The TB incidence number: 10.7 M; New cases per 100,000 population: 131; 8 high burden countries, including China, account for 87% of new global TB cases; MDR/RR-TB incidence number: 390,000; Cases per 100,000 population: 4.8.	The TB incidence number: 696,000; New cases per 100,000 population: 49; High-burden country: contributes 6.5% of global incident cases; MDR/RR-TB incidence number: 28,000; Cases per 100,000 population: 2.0; A top-2 MDR/RR-TB burden country, 7.1% of global cases.
Diagnosis & Treatment	Rapid diagnostic (molecular) coverage: 54%; Bacteriological confirmation rate: 64%; New or relapse TB treatment success rate: 88%; DST coverage among bacteriologically confirmed TB cases: 83%; MDR/RR-TB treatment success rate: 71%.	Rapid diagnostic (molecular) coverage: 87%; Bacteriological confirmation rate: 73% (below the optimal target); New or relapse TB treatment success rate: 95%; DST coverage among bacteriologically confirmed TB cases: 90%; MDR/RR-TB treatment success rate: 68%.
Prevention & Screening	The gap (the number of unreported cases) is 2,370,610 cases, with a case detection rate of 78%. Active case-finding is essential to close detection gaps; TPT coverage among household contacts: 25%.	The gap is 164,903 cases, with a case detection rate of 76%. The number in China is substantial, accounting for nearly 6.9% of the global total gap. Active case-finding is essential to close detection gaps; TPT coverage among household contacts: 2%.
Financing	82% of NTP funds from domestic sources.	100% of NTP funds from domestic sources.
UHC & Multisectoral Accountability	The UHC SCI is 68; The proportion of TB households facing catastrophic costs is 47%.	The UHC SCI is 80: China lacks nationally representative data on the proportion of TB households facing catastrophic costs.
Research & Innovation	Emphasis on new tools: vaccines, shorter regimens, novel diagnostics; 18 TB vaccine candidates are in clinical trials.	Active in operational research and adoption of new diagnostics; two TB vaccine candidates are in clinical trials.

Abbreviation: TB=tuberculosis; MDR/RR-TB=multidrug-resistant/rifampicin-resistant tuberculosis; DST=drug susceptibility testing; TPT=tuberculosis preventive treatment; NTP=national tuberculosis program; UHC=universal health coverage; SCI=service coverage index.

diagnosis and ensures that the most effective treatment regimen is selected as early as possible (*2–4*). Globally, the use of WHO-recommended rapid diagnostic tests (WRDs) increased from 48% in 2023 to 54% in 2024, driven by strong promotion in high-burden countries, including China. Through large-scale deployment of rapid molecular diagnostics, China has become one of the few high-burden countries where the initial utilization rate of rapid diagnostic technologies exceeds 80%. Drug susceptibility testing (DST) coverage among bacteriologically confirmed TB cases has reached 90%, surpassing the global average of 83%. These achievements provide a solid foundation for early and accurate diagnosis and offer a replicable model for countries with comparable resources (*5–7*).

Global comparisons also reveal a key shortcoming: China's bacteriological positivity rate remains below 75% (*8–9*). Only six high-burden countries have achieved a rate of 75% or higher. Bacteriological confirmation is the "gold standard" for TB diagnosis. The relatively low rate indicates gaps in translating advanced screening technologies into comprehensive, high-quality laboratory confirmation capacity. This challenge reflects not only technology coverage but also primary-level laboratory capacity, quality assurance systems, and sample processing efficiency. It represents a common bottleneck among high-burden countries, including China (*10*).

In the core area of case detection, China continues to face significant challenges common to many high-burden countries. It is among the top five contributors to the global gap between estimated incidence and notified cases, accounting for 6.9% of this gap. This implies that a substantial number of infectious cases remain undetected within communities, sustaining transmission (*11–12*). This gap highlights the limitations of passive case-finding strategies and reinforces the global urgency of transitioning to active case-finding.

Another challenge lies in the treatment of drug-resistant TB. While China has achieved a 95% treatment success rate for new and relapse TB cases, the success rate for RR/MDR-TB remains at 68%, below the global average of 71%. Furthermore, long-term regimens continue to predominate in China, even as global practice shifts toward all-oral short-course treatments.

China's TB Funding Model and Universal Health Coverage Amid Changes in the Global Landscape

Funding is the lifeline for the sustainable development of TB programs. Recent reductions in

international donor funding have made political commitment and domestic financing in high-burden countries more critical than ever. The global TB funding gap remains substantial, with available funds in 2024 amounting to only US$5.9 billion, less than one quarter of the annual target (US$22 billion).

In this context, China's funding model provides an important reference. In 2024, all funding for China's national TB program (NTP) was derived from domestic sources (*1*,*13*). Although still insufficient to meet actual needs, this funding structure ensures the stability and sustainability of the NTP.

However, national-level fiscal resilience has not been fully translated into household-level financial protection. Although China has made significant progress in its Universal Health Coverage (UHC) Service Coverage Index (SCI), the proportion of households facing catastrophic health expenditures (defined as out-of-pocket payments ≥10% of total household consumption) remains relatively high (*14*–*15*). This indicates that TB-related direct and indirect costs, including diagnosis and treatment, transportation, nutrition, and income loss, continue to impose a substantial financial burden on affected households (*16*–*17*). This challenge, while not unique to China, underscores the global importance of strengthening social protection mechanisms to achieve health equity and represents a key area for China's subsequent efforts.

International Experience and the Global Significance of China's Practice

In some aspects of TB control, China has transitioned from a "learner" to an "exporter of experience." The systematic scale-up of TPT in China was featured as one of the four highlighted topics in *the Report*, demonstrating the practical value of its strategy to identify high-risk populations, such as household contacts and people living with HIV (*18*–*19*), and control TB incidence at its source through TPT (*20*–*22*). Since 2021, with support from WHO, China has established a strong national framework for TPT implementation and scale-up. Key milestones include: the development of technical guidelines by the Chinese Center for Disease Control and Prevention in 2021 (*23*); issuance of national guidelines in 2023 (*24*); inclusion of TPT coverage targets for household contacts in the National Tuberculosis Prevention and Control Plan (2024–2030), specifically 60% by 2025 and 80% by 2030 (*25*); and expansion of the Zero TB Communities initiative (*26*). A standardized individual-level registration and reporting system for TPT is also being established to monitor progress and support evidence-based program refinement. The Jiangsu provincial case study exemplifies the successful implementation of this comprehensive approach, demonstrating a sustainable and scalable model for TPT expansion. However, TPT coverage among household contacts in China remains significantly below the global average. Translating this best-practice model into high nationwide coverage is a key priority for the next stage of China's TB control efforts.

FUTURE TARGETED EFFORTS BASED ON GLOBAL CONSENSUS AND CHINA'S CONTEXT

Ending the TB epidemic is a shared global vision. As underscored in *the Report*, China has made remarkable progress in TB control while continuing to face persistent challenges. *The Chinese National TB Prevention and Control Plan (2024–2030)* (*25*) provides a clear, government-led roadmap, aligned with the global End TB Strategy. China's future actions should focus on more targeted strategic investments.

Promoting the Transition from Availability to Quality in Diagnosis and Overcoming the Confirmation Rate Bottleneck

While maintaining high coverage of rapid diagnostics, it is important to implement a Laboratory Capacity Strengthening Plan focused on enhancing primary-level capabilities. The goal is to increase the bacteriological positivity rate to over 75% by strengthening specimen collection, sputum culture capacity, drug susceptibility testing, and quality assurance at all levels, ensuring that diagnostic quality aligns with international gold standards. For patients with no or scanty sputum, some provinces have used tongue swab testing and *Mycobacterium tuberculosis* enrichment techniques to improve the bacteriological positivity rate (*27*–*28*).

Shifting from Passive to Active Case Finding to Close the Detection Gap

China must aim to reduce the 6.9% global detection

gap by scaling up active case-finding strategies nationwide. Innovative approaches such as mobile clinics and digital health technologies to conduct targeted screening among high-risk groups, including older adults, people with diabetes, remote populations, and residents of high-burden regions, can be adopted. At the primary level, computer-aided diagnostic (CAD) tools have opened new pathways for the precise diagnosis of pulmonary TB (*29–31*). In the future, wider application of computer-aided whole-smear screening systems, already validated in clinical trials, may enhance diagnostic capacity at the primary level (*32*). Between 2022 and 2024, China expanded its TB-free community pilot sites from 36 to 790 (*1*), promoting active case finding through a community-based comprehensive intervention system. Sustained implementation of this strategy is required to achieve the goal of ending TB (*33–34*).

Integrating Resources to Build a Robust Response to DR-TB

DR-TB control should be positioned as a national public health priority. Expanding rapid drug-resistance screening to all presumptive TB patients, ensuring access to all-oral short-course treatment regimens, and establishing interdisciplinary patient support systems could improve treatment adherence and outcomes.

Strengthening Social Support to Create a "Firewall" Against Patient Financial Risk

Social support can be strengthened by increasing outpatient reimbursement rates for TB patients, particularly those with DR-TB, including coverage under special outpatient medical insurance schemes. Subsidies can be explored for transportation and nutrition during diagnosis and treatment. Through multisectoral collaboration, China can reduce the proportion of households facing catastrophic expenditures, thereby advancing both health and social protection.

Advancing Innovation in Preventive Treatment to Reduce Transmission at the Source

Building on existing progress, China should continue to expand TPT coverage among close contacts, people living with HIV, and other high-risk groups. At the same time, promoting the development and adoption of shorter, more patient-friendly TPT regimens to improve acceptability and strengthen source control is essential.

Establishing Cross-sectoral Collaboration Mechanisms

China has begun to develop shared data systems between hospitals and CDC institutions, enabling the capture of key information such as TB-related symptoms and test results. It also facilitates early detection and timely referral for standardized treatment. Further integration with systems for medical insurance, education, and financial assistance is needed to support precision TB control and comprehensive patient care through cross-sectoral collaboration.

CONCLUSION

The WHO Global Tuberculosis Report 2025 highlights both the achievements and leadership potential of China's TB control efforts, while revealing the substantial challenges that remain. China's experience reflects the broader global context of TB control, where technological advances coexist with systemic constraints and strong national commitment contrasts with persistent household-level risks. Having established leadership in diagnostics, China's future progress will depend on addressing key priorities: improving the bacteriological positivity rate, expanding TPT among high-risk populations, strengthening active case finding, improving DR-TB control, and reducing patient financial burden. By focusing on these strategic priorities, China can accelerate domestic progress and make a more substantial contribution to the global End TB agenda.

Conflicts of interest: The authors declare no conflicts of interest.

Funding: This research was supported by two sources: Prestandardization Research Project of the Chinese Center for Disease Control and Prevention (BZ2025-Q007); Henan Provincial Scientific and Technology Research Project for Key Project of Disease Control and Prevention (HNCDCZD20250215). The funders had no role in the study design, data collection, analysis, interpretation of the data, or writing of the manuscript.

doi: 10.46234/ccdcw2026.108

[#] Corresponding author: Linqi Diao, lqdiao@163.com.

[1] Henan Key Laboratory of Infectious Pathogenic Microbiology, Henan Provincial Center for Disease Control and Prevention, Zhengzhou City, Henan Province, China.

Submitted: November 26, 2025
Accepted: March 25, 2026
Issued: May 22, 2026

REFERENCES

1. World Health Organization. Global tuberculosis report 2025. Geneva: World Health Organization. 2025. https://www.who.int/teams/global-programme-on-tuberculosis-and-lung-health/tb-reports/global-tuberculosis-report-2025. [2025-11-12].
2. WHO. WHO consolidated guidelines on tuberculosis: module 3: diagnosis. Geneva: World Health Organization. 2025. https://www.who.int/publications/i/item/9789240107984. [2025-8-5].
3. WHO. WHO consolidated guidelines on tuberculosis: module 4: treatment and care. Geneva: World Health Organization. 2025. https://www.who.int/publications/i/item/9789240107243. [2025-4-23].
4. WHO. WHO consolidated guidelines on tuberculosis: module 5: management of tuberculosis in children and adolescents. Geneva: World Health Organization. 2022 https://www.who.int/publications/i/item/9789240046764. [2022-3-18].
5. Ma YZ, Dai XQ, Li RZ, Chi SJ, Gao JG, Liu XR, et al. Application of molecular biology to enhance the detection of infectious tuberculosis in general hospitals. Hebei Med J 2024;46(12):1890 – 3. https://doi.org/10.3969/j.issn.1002-7386.2024.12.028.
6. Yu Q, Liu HC, Zhao AL, Yu N, Zhang AJ, Xu W, et al. Optimization and combination of pulmonary tuberculosis detection methods in primary laboratories. Pract Prev Med 2023;30(3):365-8. http://dx.doi.org/10.3969/j.issn.1006-3110.2023.03.029. (In Chinese).
7. Zhang RQ, Bao XD, Bao FJ, Teng C, Xu DF, Liu Z, et al. Evaluation of the Xpert MTB/XDR test for detection of isoniazid, fluoroquinolones, and second-line injectable drugs resistance to *Mycobacterium tuberculosis*—Anhui Province, China. PLoS One 2025;20(9):e0331264. https://doi.org/10.1371/journal.pone.0331264.
8. Ruan YZ, Zhang HW, Li YH, Ma YZ, Cheng SM, Fan HY, et al. Analysis of the effect of GeneXpert MTB/RIF technology on early detection of bacteriologically confirmed and drug-resistant pulmonary tuberculosis in general hospitals. Chin J Antituberc 2023;45(11):1072 – 7. https://doi.org/10.19982/j.issn.1000-6621.20230313.
9. Zhao AL, Yu Q, Yu N, Zhang AJ, Xia H, Xu W. The value of GeneXpert MTB/RIF in improving the laboratory confirmed pulmonary tuberculosis and rifampicin resistance screening at district level institution in Beijing. Chin J Antituberc 2023;45(11):1064 – 71. https://doi.org/10.19982/j.issn.1000-6621.20230206.
10. Song YY, Xia H. Survey on satisfaction of external quality assessment among tuberculosis laboratory network in China. Chin J Antituberc 2023;45(6):559 – 65. https://doi.org/10.19982/j.issn.1000-6621.20230013.
11. Fan MK, Liu YS, Li T, Liu K, Li YH, Liu XQ, et al. Analysis of the differences and influencing factors between the actual and predicted incidence numbers pulmonary tuberculosis in China from 2020 to 2022. Chin J Front Med Sci (Electron Version) 2025;17(4):57 – 63. https://doi.org/10.12037/YXQY.2025.04-09.
12. Ybryim A, Li YH, Li T, Liu XQ, Zhang H. The underdiagnosis and risk factors of pulmonary tuberculosis in non-designated medical institutions. Chin J Front Med Sci (Electron Version) 2024;16(3):16 – 21. https://doi.org/10.12037/YXQY.2024.03-04.
13. Zhou WY, Wen ZX, Gao MX, Li T, Zhang H, Wang WB. Prediction of the effectiveness and impact of the free healthcare policy for tuberculosis in China. Chin J Antituberc 2023;45(9):845 – 56. https://doi.org/10.19982/j.issn.1000-6621.20230143.
14. Hao DQ, Li T, Huang F, Xu CH. A cross-sectional study on the economic burden of pulmonary tuberculosis patients from western China. Chin J Antituberc 2023;45(11):1021 – 30. https://doi.org/10.19982/j.issn.1000-6621.20230137.
15. Xu CH, Xia YY, Hu DM, Zhang XM, Zhao YL. Financial burden of tuberculosis patients - China, 2020. China CDC Wkly 2023;5(12):266 – 70. https://doi.org/10.46234/ccdcw2023.048.
16. Liu YH, Gao MQ, Zhang LJ, Ma LP, Nie LH, Jiang GL, et al. Estimation on direct medical costs of pulmonary tuberculosis in China. Chin J Antituberc 2023;45(12):1134 – 40. https://doi.org/10.19982/j.issn.1000-6621.20230317.
17. Wang BN, Gao ZD, Xu Y, Li T, Ruan YZ, Chen W, et al. Study of self-paid medical expenses of drug-resistant tuberculosis patients and influencing factors in Beijing, 2021–2023. Dis Surveill 2025;40(7):949 – 56. https://doi.org/10.3784/jbjc.202412020694.
18. Gao L, Zhang H, Hu MG, Xu CD, Xia YY, Li T, et al. Estimation of the national burden on latent tuberculosis infection based a multi-center epidemiological survey and the space statistics model. Chin J Antituberc 2022;44(1):54 – 9. https://doi.org/10.19982/j.issn.1000-6621.20210661.
19. Ma Y, Lu W, Gao L, Chu NH, Zhou L, Cheng SM. To end tuberculosis epidemic needs strengthen the management of screening and preventive treatment of latent tuberculosis infection in high-risk groups. Chin J Antituberc 2022;44(3):209 – 14. https://doi.org/10.19982/j.issn.1000-6621.20220008.
20. Xu CH, Zhao YL. China's countermeasures in the context of Global Tuberculosis Prevention Action. Chin J Tuberc Respir Dis 2022;45(3):308 – 12. https://doi.org/10.3760/cma.j.cn112147-20210722-00520.
21. Fa LF, Xu CH, Cheng J, Zhang H. Acceptability of tuberculosis preventive treatment strategies among healthcare workers using an online survey - China, 2021. China CDC Wkly 2022;4(11):211 – 5. https://doi.org/10.46234/ccdcw2022.050.
22. Du R, Xiao X, Chen J, Shen X, Zhao Q. Epidemiological analysis of tuberculosis infection and trend changes - 152 belt and road partner countries, 2013-2021. China CDC Wkly 2024;6(49):1289 – 93. https://doi.org/10.46234/ccdcw2024.257.
23. National Health Commission of the People's Republic of China. Technical Specification for Tuberculosis Prevention and Control in China (2020 Edition) https://tb.chinacdc.cn/ggl/202004/P020200414515703939844.pdf. [2020-4-2].
24. Xu CH, Zhao YL. China national guidelines on tuberculosis preventive treatment. Beijing: People's Medical Publishing House. 2023. http://find.nlc.cn/search/showDocDetails?docId=-5905194106695645092&dataSource=ucs01&query=%E4%B8%AD%E5%9B%BD%E7%BB%93%E6%A0%B8%E7%97%85%E9%A2%84%E9%98%B2%E6%80%A7%E6%B2%BB%E7%96%97%E6%8C%87%E5%8D%97. (In Chinese).
25. National Disease Control and Prevention Administration, National Health Commission, National Development and Reform Commission, et al. Notice on issuing the "national tuberculosis prevention and control plan (2024-2030)". 2024. https://www.gov.cn/zhengce/zhengceku/202412/content_6991217.htm.
26. Xu CH, Zhao YL. Commit, invest and deliver: towards achieving end tuberculosis strategy goals through active case finding and preventive treatment in China. China CDC Wkly 2025;7(13):407 – 12. https://doi.org/10.46234/ccdcw2025.068.
27. Huang MS, Wu YN, Li GL, Liu HC. Research advances of *Mycobacterium tuberculosis* enrichment technology. Chin J Antituberc 2025;47(3):369 – 73. https://doi.org/10.19982/j.issn.1000-6621.20240420.
28. Dong Y, Pang Y. Focusing on the diagnosis of pulmonary tuberculosis in sputum-free patients and exploring the potential of tongue swab substitution. Chin J Antituberc 2023;45(12):1131 – 3. https://doi.org/10.19982/j.issn.1000-6621.20230379.
29. Nijiati M, Abudukaiyoumu A, Damaola M, Abulizi A, Tian XW, Dai

GC. Application value of pulmonary tuberculosis screening technology based on artificial intelligence in image diagnosis of primary hospital. Electron J Emerg Infect Dis 2021;6(2):138 – 42. https://doi.org/10.19871/j.cnki.xfcrbzz.2021.02.014.
30. Wang YF, Sun YB, Yan XL, Cao Y, Liu C, Qi Z, et al. Application value of digital X-ray chest radiography artificial intelligence aided diagnosis system in tuberculosis screening. Chin J Public Health Manage 2022;38(6):871 – 4. https://doi.org/10.19568/j.cnki.23-1318.2022.06.0041.
31. Wang XL, Wang XW, Lei J, Liu T, Lu JR, Tian XM, et al. Application of artificial intelligence image screening system for tuberculosis in Ningxia autonomous region. China Digital Med 2020;15(4):39 – 41. https://doi.org/10.3969/j.issn.1673-7571.2020.04.012.
32. Law YN, Jian HB, Lo NWS, Ip M, Chan MMY, Kam KM, et al. Low cost automated whole smear microscopy screening system for detection of acid fast bacilli. PLoS One 2018;13(1):e0190988. https://doi.org/10.1371/journal.pone.0190988.
33. Cheng J, Zhao YL. Screening strategy in zero tuberculosis community project. Chin J Antituberc 2024;46(6):605 – 12. https://doi.org/10.19982/j.issn.1000-6621.20230435.
34. Sun JW, Gao M, Zhao AH, Zhang P, Li MJ, Sun DY. First year evaluation of a Tuberculosis-free communities pilot program in Henan Province: a key indicator analysis. Mod Dis Control Prev 2026;37(2):87 – 92. https://doi.org/10.13515/j.cnki.hnjpm.1006-8414.2026.02.002.

Youth Editorial Board

Indexed by Science Citation Index Expanded (SCIE), Social Sciences Citation Index (SSCI), PubMed Central (PMC), Scopus, Chinese Scientific and Technical Papers and Citations, and Chinese Science Citation Database (CSCD)

The inauguration of *China CDC Weekly* is in part supported by Project for Enhancing International Impact of China STM Journals Category D (PIIJ2-D-04-(2018)) of China Association for Science and Technology (CAST).

CHINA CDC WEEKLY

CCDC weekly

Vol. 8 No. 21 May 22, 2026

中国疾病预防控制中心周报(英文)

Responsible Authority
National Disease Control and Prevention Administration

Sponsor
Chinese Center for Disease Control and Prevention &
Chinese Academy of Preventive Medicine

Editor-in-Chief
Jianwei Wang

Editing and Publishing
China CDC Weekly Editorial Office
No.155 Changbai Road, Changping District, Beijing, China
Tel: 86-10-63150501, 63150701
Email: weekly@chinacdc.cn

Printing: Beijing Kexin Printing Co., Ltd

Complimentary Access

CSSN
ISSN 2096-7071 (Print)
ISSN 2097-3101 (Online)
CN 10-1629/R1